

Short Review Article

Advanced dual-atom catalysts for rechargeable zinc-air batteries

Xiaorong Lin, Gao Chen ^{*}, Yanping Zhu, Haitao Huang ^{**}

Department of Applied Physics and Research Institute for Smart Energy, The Hong Kong Polytechnic University, Hung Hom, Hong Kong, China

ARTICLE INFO

Keywords:

Dual-atom catalysts
Bifunctional oxygen electrocatalysis
Zinc-air batteries
Solid-state zinc-air batteries

ABSTRACT

Rechargeable zinc-air batteries (ZABs) have gained extensive research attention as a promising sustainable energy technology due to their considerable theoretical specific energy density, low toxicity, abundant availability, and robust safety features. However, the practical implementation of ZABs still faces challenges, primarily attributed to the sluggish kinetics of oxygen-involved reactions, including oxygen reduction reaction (ORR) and oxygen evolution reaction (OER) during the discharge and charge process. Therefore, searching for efficient bifunctional oxygen electrocatalysts is crucial to address these challenges. Dual-atom catalysts (DACs), an extension of single-atom catalysts (SACs), exhibit flexible architectures that allow for the combination of homogeneous and/or heterogeneous active sites, making them highly attractive for improving bifunctional activity. In this review, we first introduce the basic framework of ZABs and the structural characteristics of DACs. Subsequently, we organize the research progress on applying DACs in liquid and solid-state ZABs and elaborate on their unique catalytic mechanism. Finally, we highlight the challenges and future research directions for further innovation of DACs in ZABs. In summary, this review highlights the advantages of DACs compared with SACs used as bifunctional oxygen electrocatalysts and provides a reference for the broad applications of DACs in energy conversion and storage.

1. Introduction

With the growing concerns about energy and environment, extensive endeavors have been devoted to the pursuit of greener and more sustainable energy storage devices [1–6]. Among the various options available, lithium-ion batteries (LIBs) have long dominated the market due to their considerable energy density [7–9]. Nonetheless, the high cost of the raw materials as well as safety concerns pose obstacles to their further implementation for large-scale energy storage devices [10–12]. To address these concerns, researchers have turned their attention to rechargeable zinc-air batteries (ZABs). Composed of Zn anode, air cathode, electrolyte, and separator, ZABs offer a theoretical specific energy density 2.5 times higher than that of LIBs [13,14]. Moreover, the abundance of Zn in the Earth's crust, coupled with the advantages of prolonged discharge duration, stability, and operational safety, positions ZABs as a highly promising alternative to LIBs [15]. Traditionally, liquid-state systems with alkaline electrolyte solutions have been widely used in ZABs. However, the increasing demand for portable and wearable electronics has spurred the development of flexible solid-state ZABs based on (semi-)solid electrolytes have gained widespread attention [16,

17]. Compared with traditional liquid-state ZABs, solid-state ZABs offer enhanced versatility and superior mechanical strength, thus driving extensive research in this field. Either liquid or solid-state ZABs face challenges related to the sluggish kinetics of the oxygen reduction reaction (ORR) and oxygen evolution reaction (OER) occurring at the air cathode. These limitations result in high overpotentials, poor cycling stability, and low power density, thereby impeding the large-scale advancement of ZABs [18–20]. State-of-the-art electrocatalysts based on noble metals such as Pt/C for ORR and IrO₂ for OER have been widely used. However, their exorbitant cost, limited reserves, and poor durability impede their industrial-scale production for ZABs. Consequently, substantial efforts have been dedicated to the development of efficient and cost-effective oxygen electrocatalysts, particularly those with bifunctional catalytic activity.

The field of single-atom catalysts (SACs) emerged in 2011 with the pioneering work of Zhang et al. [21]. Since then, SACs have gained widespread attention across various fields due to their nearly 100% utilization of metal atoms, resulting in excellent activity and selectivity in a wide range of applications [22–26]. However, SACs also exhibit certain limitations and shortcomings [27]. Firstly, single metal atoms are prone

^{*} Corresponding author.^{**} Corresponding author.E-mail addresses: gaochen@polyu.edu.hk (G. Chen), aphuang@polyu.edu.hk (H. Huang).

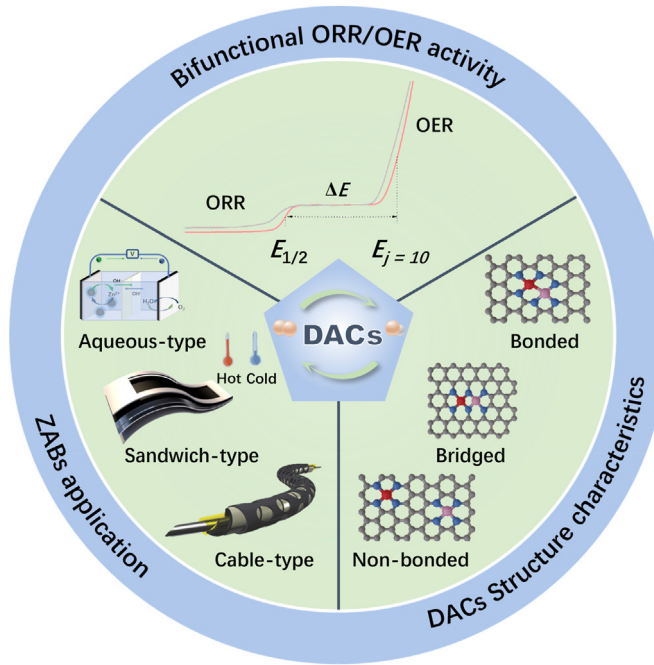


Fig. 1. Schematic diagram of the application of DACs as bifunctional catalysts in ZABs.

to aggregation due to their high specific surface energy, so the metal loading is usually kept at a low level to ensure the effective distribution of isolated active sites, thus weakening the overall activity [28,29]. Secondly, since most SACs only possess a single type of specific active site, making it challenging to break the linear scaling relationship between intermediates in complex reactions involving multiple intermediates [30]. Moreover, a single active site faces difficulties in catalyzing multi-step reactions or developing bifunctional catalysts involving multiple active sites. To overcome these challenges, dual-atom catalysts (DACs) have emerged as an extension of SACs, offering several advantages. DACs exhibit higher metal loading and flexible active sites that can adjust the *d*-band center through the electron orbitals interaction, thereby optimizing the adsorption energy of intermediates on the active

sites [31]. Given the tremendous potential of DACs and the need for developing bifunctional oxygen electrocatalysts for ZABs, a growing number of publications have focused on this area. Although several reviews have been published on the synthesis, characterizations, and electrochemical applications of DACs [32–35], to the best of our knowledge, no review has specifically addressed DACs as bifunctional oxygen electrocatalysts for ZABs. Therefore, a comprehensive evaluation of the utilization of DACs in the realm of ZABs is urgently needed. This review aims to emphasize the structural characteristics of DACs, elucidate the atomic interactions within DACs, and provide an overview of the current application status of DACs in both liquid and solid-state ZABs. Furthermore, a concise summary and outlook are provided regarding the implementation of DACs in ZABs, along with the identification of critical issues and future development directions for DACs (Fig. 1).

2. Fundamentals of ZABs and oxygen electrocatalysts

2.1. Configuration of ZABs and ORR/OER reaction mechanisms

Rechargeable ZABs are complex electrochemical systems consisting of four main components: an air cathode, a metal Zn anode, an electrolyte and an electrically insulating separator. Based on the electrolyte type and battery structure employed, current ZABs can be categorized into four main types: aqueous-type [36], sandwich-type [36], cable-type [37], and all-solid-state ZABs (Fig. 2) [38]. The latter three varieties utilize (semi-) solid electrolytes, are collectively referred to as solid-state ZABs [39–41]. Table 1 illustrates the redox reactions that occur on ZABs during the charge and discharge processes.

The air cathode plays a crucial role in catalyzing ORR and OER during ZABs' working process, which in turn directly determines the round-trip efficiency and power density of ZABs. Therefore, it is essential to have a comprehensive understanding of the mechanisms involved in ORR and OER to design high-performance bifunctional catalysts [42]. According to the electron transfer number, ORR can be divided into two categories, namely two-electron and four-electron transfer processes. The two-electron reduction process primarily produces hydrogen peroxide, which can react with the active materials in ZABs, leading to decreased battery efficiency and lifespan [43–45]. Therefore, the four-electron pathways for the ORR are highly preferred for ZABs due to its higher oxygen utilization efficiency and potential for higher energy conversion

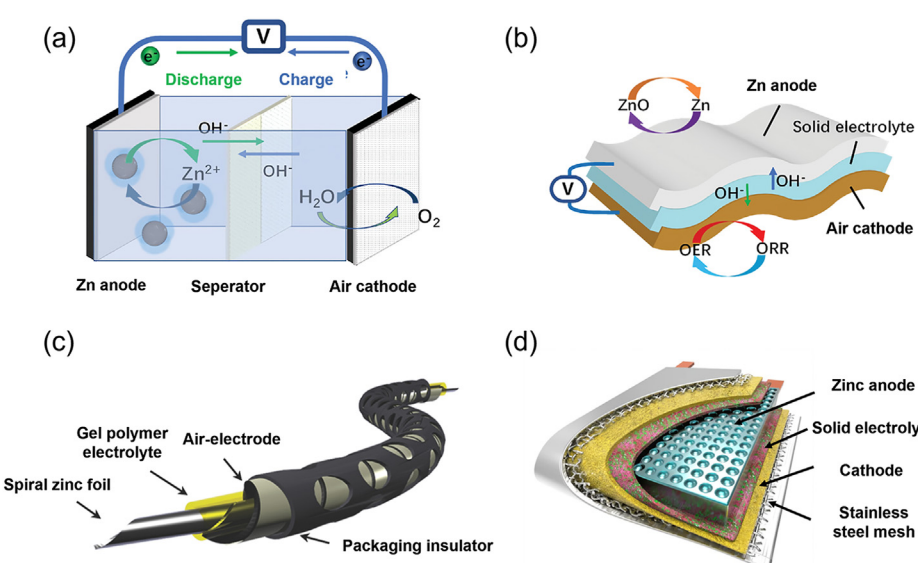


Fig. 2. (a) Schematic illustration of aqueous-type ZABs. (b) Schematic illustration of sandwich-type ZABs. Reprinted with permission from Ref. [36]. Copyright 2020 John Wiley & Sons. (c) Schematic illustration of cable-type ZABs. Reprinted with permission from Ref. [37]. Copyright 2014 John Wiley & Sons. (d) Schematic illustration of all-solid-state zinc-air pouch cell. Reprinted with permission from Ref. [38]. Copyright 2021 Springer Nature.

Table 1

Discharge and charge reactions of Zn anodes in ZABs.

	Discharge Reactions	Charge Reactions
Zn anode	$\text{Zn} + 4\text{OH}^- \rightarrow \text{Zn(OH)}_4^{2-} + 2e^-$	$\text{Zn(OH)}_4^{2-} + 2e^- \rightarrow \text{Zn} + 4\text{OH}^-$
Air cathode	$\text{Zn(OH)}_4^{2-} \rightarrow \text{ZnO} + \text{H}_2\text{O} + 2\text{OH}^-$	$\text{ZnO} + \text{H}_2\text{O} + 2\text{OH}^- \rightarrow \text{Zn(OH)}_4^{2-}$
Overall reactions	$\text{O}_2 + 2\text{H}_2\text{O} + 4e^- \rightarrow 4\text{OH}^-$ $2\text{Zn} + \text{O}_2 \rightarrow 2\text{ZnO}$	$4\text{OH}^- \rightarrow \text{O}_2 + 2\text{H}_2\text{O} + 4e^-$ $2\text{ZnO} \rightarrow 2\text{Zn} + \text{O}_2$

Table 2

Reaction pathways and overall reactions of ORR and OER in ZABs.

ORR	OER
$* + \text{O}_2 + \text{H}_2\text{O} + e^- \rightarrow \text{OOH}^* + \text{OH}^-$	$* + \text{OH}^- \rightarrow \text{OH}^* + e^-$
$\text{OOH}^* + e^- \rightarrow \text{O}^* + \text{OH}^-$	$\text{OH}^* + \text{OH}^- \rightarrow \text{O}^* + \text{H}_2\text{O} + e^-$
$\text{O}^* + \text{H}_2\text{O} + e^- \rightarrow \text{OH}^* + \text{OH}^-$	$\text{O}^* + \text{OH}^- \rightarrow \text{OOH}^* + e^-$
$\text{OH}^* + e^- \rightarrow * + \text{OH}^-$	$\text{OOH}^* + \text{OH}^- \rightarrow * + \text{O}_2 + \text{H}_2\text{O} + e^-$

Note: * represents the catalytic site of the catalysts and OOH^* , O^* , and OH^* are the intermediates adsorbed on the catalytic sites.

efficiency. **Table 2** provides an illustration of the reaction pathways for ORR in ZABs, involving oxygen diffusion to the catalyst surface, followed by its adsorption process. Subsequently, the oxygen bond is weakened and broken by electrons transferred from the anode, resulting in the release of hydroxyl ions into the electrolyte from the catalyst surface [46].

OER, as the reverse process of ORR, is initiated with the adsorption of and followed by two possible mechanisms [47]. One is the lattice-oxygen-mediated mechanism (LOM), which involves direct formation of O_2 through coupling between lattice oxygen and O^* . However, this mechanism usually creates oxygen vacancies leading to poor catalyst durability and structural evolution issues [48]. The other is the adsorbate evolution mechanism (AEM), where the oxygen precursor undergoes a stepwise process of adsorption, deprotonation, coupling, and desorption. This pathway is completely opposite to the four-electron ORR pathway illustrated in the previous equation. Hence, OER may follow the AEM as depicted in **Table 2**. It is evident that both ORR and OER are complex processes involving various surface intermediates and multi-step electron-transfer processes. The intricate mechanism and sluggish kinetics of the main four-electron pathways necessitate high overpotentials to drive these reactions, thereby reducing overall energy efficiency of ZABs. This presents a significant challenge to the practical deployment of ZABs. Therefore, the design of efficient oxygen electrocatalysts is crucial to promote the practical application of ZABs.

Since the reaction pathways of ORR and OER are different, their requirements for catalytic active sites are also distinct. The ORR activity is primarily limited by the OH^* reduction step and the oxygen reduction steps, while the OER activity is restricted by the OOH^* and O^* formation steps [49,50]. Therefore, when designing catalysts for ORR and OER, it is necessary to incorporate active sites that can effectively adsorb and activate OH^* and OOH^*/O^* intermediates [51]. Recent studies have demonstrated that DACs exhibit enhanced oxygen electrocatalysis compared with SACs [31,52]. This improvement can be attributed to the special structural characteristics of DACs, including increased number of active sites and improved intermediate adsorption activity. DACs maximize the potential of SACs in multi-step reactions such as ORR and OER while allowing for activity and selectivity adjustments, which provides a new avenue for designing bifunctional catalysts. The application of DACs has led to significant advancements in the performance of ZABs, which will be further discussed in Section 3, detailing the breakthroughs in DACs development for ORR/OER electrocatalysis.

2.2. Evaluation parameters of oxygen electrocatalysts

The use of electrocatalysts can accelerate the reaction kinetics of ORR and OER in the air cathode. Several crucial parameters and electro-

chemical measurement routes are employed to evaluate the catalytic activity of oxygen electrocatalysts. The catalytic performance of electrocatalysts is typically examined in a three-electrode system to obtain important parameters such as overpotential (the difference between practical potential and the theoretical equilibrium potential of the electrode), electron transfer number, Tafel slope and stability [36,53]. Furthermore, the combination of rotating disk electrode (RDE) and/or rotating ring disk electrode (RRDE) techniques enables the acquisition of ORR kinetic information, such as overall electron transfer number and exchange current density. For oxygen reactions involving multi-step electron transfer processes, a large overpotential is required to overcome the energy barrier during the reaction. Therefore, overpotential is one of the fundamental criteria for assessing catalyst performance. In catalyst design, lower overpotential values are more suitable for enhancing the utilization efficiency of electric energy. The diffusion limiting current density, which represents the maximum current density that ORR can reach at a specific disk/ring speed, is a criterion for ORR. The larger value provides a larger current value passing through per unit area, thus speeding up the reaction kinetics [54]. The onset potential (E_{onset}) refers to the potential at which the current deviates from the background current under an argon atmosphere and half-wave potential ($E_{1/2}$, potential at one-half of the diffusion limiting current density) are regarded as important criterion for evaluating the ORR performance of the electrocatalysts. A higher $E_{1/2}$ reflects a lower overpotential value thus signifying an increased catalytic activity. Moreover, the electron transfer number obtained using RDE or RRDE can be utilized to determine the dominant mechanism in the ORR.

Regarding OER, the potential at 10 mA/cm^2 ($E_{j=10}$) is an important indicator for evaluating catalytic performance. Additionally, the Tafel slope (b) is another criterion used for accessing OER activity, determined by the relationship between overpotential (η) and current density (j) in the polarization area: $\eta = a + b \log j$ [55]. A smaller Tafel slope indicates a more favorable kinetic process. The extrinsic or apparent OER activity of a catalyst depends on the specific surface area and catalyst loading, and the intrinsic activity can be obtained by further normalizing the current density to the electrochemical active surface area (ECSA) or mass loading [56]. At the same time, stability determines the lifespan of a catalyst, which is crucial for practical applications. Typically, it can be examined by using chronoamperometry or chronopotentiometry (CP) techniques.

For catalysts exhibiting ORR/OER bifunctional activity, the potential difference ΔE ($\Delta E = E_{j=10} - E_{1/2}$) is used to evaluate the overall activity, where a smaller ΔE value indicates the superior catalytic activity of the bifunctional catalyst. By designing high-performance ORR and OER catalysts, the polarization of ZABs during discharge and charge can be effectively mitigated, thereby enhancing the overall performance of the battery.

2.3. Evaluation parameters of ZABs

The performance of ZABs is an important basis for evaluating the actual performance of electrocatalysts. As energy storage devices, the performance of ZABs can be split into two aspects: their discharge properties and their rechargeability [57]. Discharge performance is characterized by the following indicators: the battery's open-circuit voltage (OCV), power density, and specific capacity. OCV refers to the voltage difference between the cathode and anode when no current is

flowing, which reflects the activity of the air cathode. Through the discharge curve (current polarization potential response under different discharge current densities), the power density is obtained by multiplying the discharge potential by the corresponding current density. The higher peak power density supports improved output performance of the device. The specific capacity is determined by discharging the battery under fixed current densities until the voltage drops to a preset cutoff value, and further normalized to the mass of Zn consumed during discharge, which can be compared with the theoretical specific capacity (820 mAh/g_{Zn}) to estimate the battery performance [58].

On the other hand, the rechargeability of ZABs is evaluated through round-trip efficiency and cycle life test. Specifically, an accelerated testing technique of Galvanostatic cycling is applied, whereby alternately applying fixed negative and positive currents, and simultaneously recording the corresponding discharge and charge voltages. The round-trip efficiency is defined as the ratio of discharge voltage to charge voltage, which represents the energy utilization efficiency of the ZABs. Therefore, efficient ORR/OER catalytic activity is beneficial to reducing the overpotentials of discharge and charge reactions, thereby improving the round-trip efficiency. For galvanostatic cycle test, the test parameters (such as current density, time length and the number of cycles) will affect the test results. Currently, standard parameters have not been established for in-lab testing of ZABs. In the future, common standards for test parameters should be established based on different battery applications, including electric vehicles, smart grids, and personal electronics [13].

3. Classification and structural characterization of DACs

3.1. Classification

For SACs, single atoms are commonly dispersed randomly and isolated from each other, resulting in a lack of interaction between active sites [59]. As an extension of the SAC family, DACs have more advantages in terms of the coordination environment and active site density [31,59]. They have become an emerging frontier by utilizing multiple active sites or synergistic effects to achieve efficient catalysis, especially for multi-step processes of OER and ORR [35,60]. Many researchers have successfully synthesized DACs with excellent catalytic properties through carefully designed strategies to regulate the electronic structure, the binding energy of the reaction intermediates or the local structural conversion, which provides an important foundation for advancing the

application and performance optimization of ZABs [61,62]. Based on the structural characteristics of DACs, they can generally be divided into three main categories: bonded, bridged, and non-bonded DACs (Fig. 3). Moreover, some catalysts cover two or three of the above structural characteristics [63–66]. By deeply understanding the structural characteristics of DACs, we can better comprehend their catalytic performance and reaction mechanisms, thereby offering guidance and inspiration for the synthesis of more efficient DACs.

3.2. Structural characterization

Precise characterization of DACs is crucial for establishing reliable structure-activity relationship and designing and optimizing catalysts for specific catalytic reactions. In recent years, several advanced characterization techniques have been employed to determine the atomic configurations and dual-atom structures of DACs. In this section, we discuss two major characterization techniques: transmission electron microscopy (TEM) and X-ray absorption spectroscopy (XAS).

TEM is a widely used tool for identifying catalyst morphology and visualizing atomic structures. Especially, the aberration-corrected high-angle annular dark-field scanning transmission electron microscopy (AC HAADF-STEM) mode has gained considerable attention in the characterization of DACs [67], which enables the identification of adjacent metal atoms and their atomic distances, as well as the evaluation of the degree of uniformity of surface species. The bimetallic catalyst atoms usually appear brighter since they have higher atomic numbers than the elements in the catalyst support (typically composed of carbon and nitrogen) [68,69]. Additionally, element-specific energy-dispersed X-ray spectroscopy (EDS) and electron energy-loss spectroscopy (EELS) can be performed to identify the chemical species of metal elements, which further aids the identification of dual-atom pairs [70]. One example shown in Fig. 4 illustrates the identification of adjacent Fe and Ni single atoms on a nitrogen-doped carbon support using AC HAADF-STEM [71]. The majority of the paired bright spots (typically enclosed in red boxes) correspond to Fe-Ni single atom pairs (Fig. 4a). Moreover, in the randomly selected regions of Fig. 4a, the atomic pairs identified based on intensity distribution exhibit distances close to 4.1 Å, confirming the formation of diatomic structures (Fig. 4b). Furthermore, EELS line scans revealed the presence of one iron atom and one nickel atom in the DACs, providing strong evidence for the formation of Fe-Ni DACs (Fig. 4c and d). This work demonstrates the application of advanced TEM techniques in the characterization of DACs.

XAS is another indispensable technique to characterize DACs, including X-ray absorption near-edge spectroscopy (XANES) and extended X-ray absorption fine structure (EXAFS). This technique can provide valuable information on the average geometric and electronic structure of single atoms. XANES is more sensitive to chemical information, such as valence states, *d*-band occupancy, and local symmetry. On the other hand, EXAFS offers valuable information regarding coordinating atoms, coordination numbers, and bond lengths [72]. In Wu et al.'s work, XAS was employed to investigate the coordination environment and electronic structure of CoIn-N-C DAC [73]. XANES analysis indicated that the oxidation state of Co is between 0 and +2, while the oxidation state of In is between 0 and +3 (Fig. 4e). EXAFS analysis further elucidated the structure of the active site (Fig. 4f). The peak at 1.4 Å corresponded to the Co-N coordination path, whereas the peak at 1.7 Å corresponded to the In-N coordination path in CoIn-N-C. Additionally, a minor peak at 2.4 Å in Co K-edge EXAFS fitting curve was observed, suggesting the presence of a paired Co-In diatomic configuration. The fitting results demonstrated that the coordination numbers of Co-N and In-N were approximately 4, while the coordination numbers of Co-In were both around 1. These results indicated that the local structure of Co-In diatomic sites is in the form of CoInN₆, as depicted in the inset of Fig. 4f. This work highlights the importance of XAS in determining the local coordination environment and atomic structure of DACs.

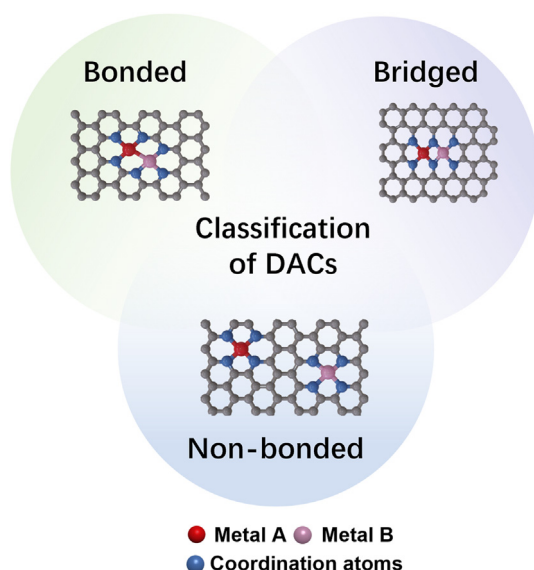


Fig. 3. Conclusive illustration of different type of DACs.

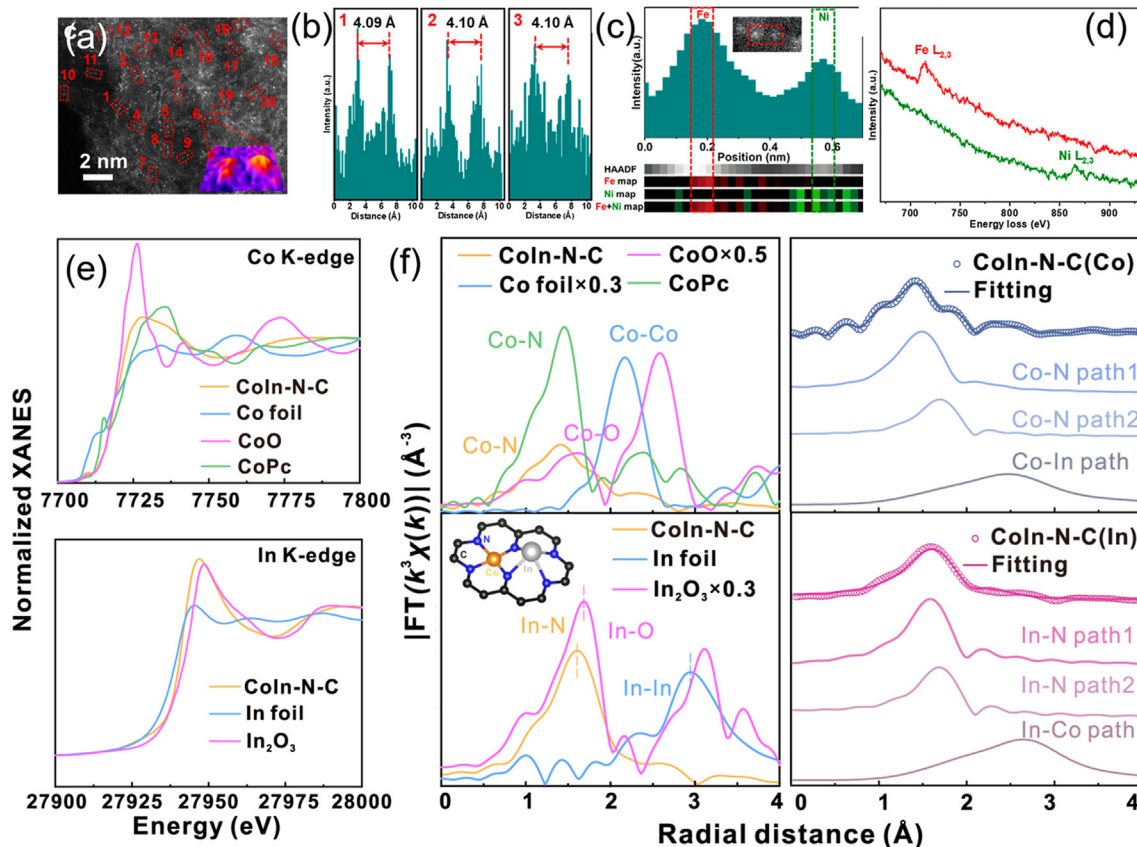


Fig. 4. (a) AC HAADF-STEM image of Fe-Ni DACs. (b) Line-scanning intensity profiles obtained from the region 1–3 highlighted in panel a. (c) Simultaneously acquired HAADF-STEM image intensity profile accompanied by EELS mapping of Fe-Ni DACs presented in panel c. (d) Single-atom EELS spectra extracted from two atomic positions highlighted in red and green in panel c. Reprinted with permission from Ref. [71]. Copyright 2021 American Chemical Society. (e) Co (top) and In (down) K-edge XANES. (f) Fourier-transform EXAFS spectra of CoIn-N-C and other reference samples (left). EXAFS fitting curves of Co and In K-edge EXAFS of CoIn-N-C (right). The left inset is the illustration of the coordination structure of CoIn-N-C. Reprinted with permission from Ref. [73]. Copyright 2023 Springer Nature.

4. Catalytic promotion effects of different types of DACs

As mentioned above, according to the different structural characteristics, DACs can be divided into three main categories. This structural diversity provides more opportunities for DACs to be explored as bifunctional oxygen electrocatalysts. Here, we discuss catalytic promotion effects of different types of DACs in specific oxygen electrocatalytic reactions.

4.1. Bonded DACs

Bonded DACs are a category of catalysts where metal active sites are directly bonded to each other, resulting in strong interactions between two neighboring metal atoms [34]. Depending on the bonding metal, DACs can be further classified into homonuclear and heteronuclear bonded DACs. Homonuclear bonded DACs, characterized by metal-metal interactions, demonstrate unique atomic configurations and coordination

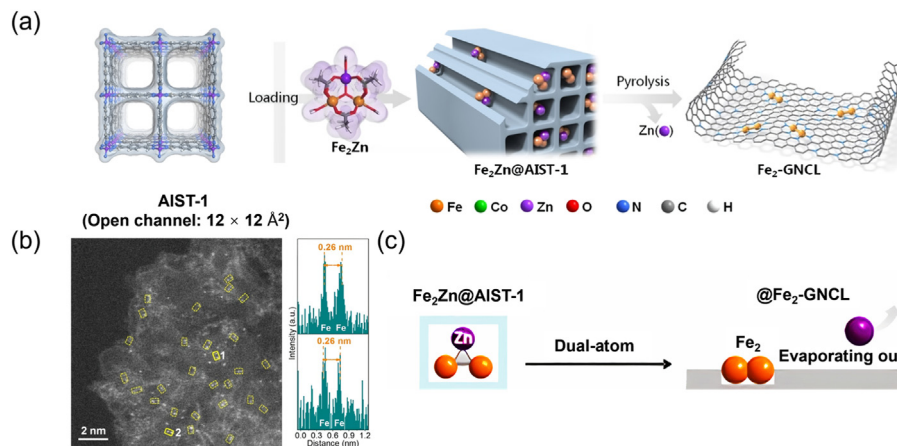


Fig. 5. Homonuclear bonded DACs as bifunctional electrocatalysts. (a) Schematic diagram of the preparation of dual-atom iron catalysts. (b) AC HAADF-STEM image of Fe₂-GNCL. Right insets are the corresponding intensity profiles from the atomic sites 1 and 2 (top and bottom, respectively). (c) The thermal clustering fashions of iron pairs in MOF encapsulated Fe₂Zn complex within the channels. Reprinted with permission from Ref. [76]. Copyright 2020 John Wiley & Sons.

environments. These distinctive characteristics facilitate the optimization of reaction intermediate adsorption, thereby significantly enhancing catalytic performance [74,75]. For example, Wei et al. have developed a “heteroatom modulator approach” to construct dual-atom iron catalysts [76]. They utilized a unique metal-organic framework (MOF) named AIST-1 as a precursor. AIST-1 is characterized by well-ordered aromatic ring arrays and abundant micropores, providing spacious channels for encapsulating a trinuclear $\text{Fe}^{\text{III}}_2\text{Zn}^{\text{II}}(\mu_3\text{-O})(\text{CH}_3\text{COO})_6(\text{H}_2\text{O})_3$ complex. Following high-temperature pyrolysis, they obtained $\text{Fe}_2\text{-GNCL}$ (Fig. 5a). The existence of dual iron atoms in $\text{Fe}_2\text{-GNCL}$ was directly confirmed by HAADF-STEM images, where numerous small bright spot pairs (highlighted in yellow boxes) were observed (Fig. 5b). The formation mechanism of homonuclear $\text{Fe}_2\text{-GNCL}$ involves the presence of Zn^{II} during the high-temperature carbonization process, effectively preventing the aggregation of Fe atoms into clusters. Subsequently, Zn evaporates, leaving stable iron dimers (Fig. 5c). Notably, intensity profiles distinctly identify dual Fe sites approximately 2.6 Å apart, indicating a strong interaction between the two atoms (Fig. 5b). Combined with reduced adsorption energies of oxygen intermediates, $\text{Fe}_2\text{-GNCL}$ exhibits lower OER overpotential compared with IrO_2 , as well as comparable ORR performance to

Pt/C . This study presents a promising strategy for designing homonuclear bonded DACs with excellent bifunctional electrocatalytic capability at atomic level. Furthermore, computational screening is an effective approach for investigating the bifunctional activity of homonuclear bonded DACs. For example, Huang et al. employed density functional theory (DFT) calculations to design a series of DACs supported on C_2N , including 30 homonuclear $\text{M}_2\text{-C}_2\text{N}$ structures, to systematically explore their electrocatalytic potential for the ORR and OER [77]. Their research revealed that $\text{Pd}_2\text{-C}_2\text{N}$ and $\text{Pt}_2\text{-C}_2\text{N}$ exhibit the most promising performance as bifunctional catalysts, owing to the well-balanced adsorption strength of reaction intermediates. This study underscores that computational screening can provide a clear framework for future DACs design. Based on the above discussion, although several homonuclear bonded DACs with satisfactory ORR or OER performance have been developed [78], more examples demonstrating bifunctional homonuclear catalysts are still lacking. Therefore, further research is required to explore homonuclear bonded DACs as outstanding bifunctional catalysts at the atomic level.

Heteronuclear bonded DACs involve the direct bonding of two distinct central metal atoms, resulting in the formation of asymmetric

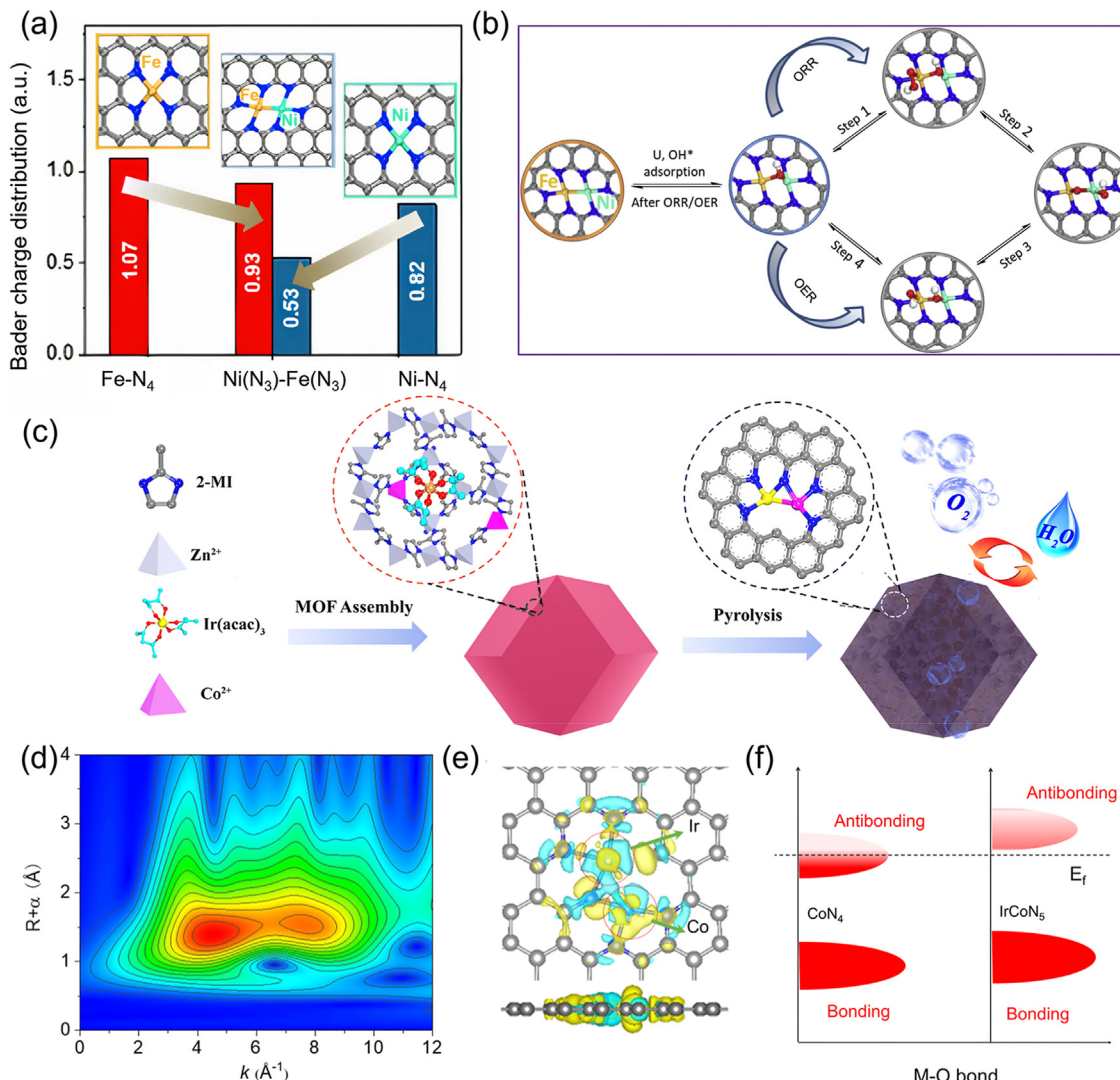


Fig. 6. Modulation effect of heteronuclear bonded DACs as bifunctional electrocatalysts. (a) Bader charge distributions for the Ni-N_4 , Fe-N_4 and $\text{Ni}(\text{N}_3)\text{-Fe}(\text{N}_3)$ moieties, with insets showing the corresponding structures. (b) Proposed ORR and OER mechanism on $\text{Ni}(\text{N}_3)(\text{OH})\text{-Fe}(\text{N}_3)\text{-C}_n$. Reprinted with permission from Ref. [80]. Copyright 2020 Elsevier. (c) Schematic diagram of the synthesis process of diatomic IrCo-N-C catalysts. (d) The EXAFS-WT of the Ir L_3 -edge for IrCo-N-C . (e) Charge density difference for IrCoN_5 . (f) Schematic representation of bond formation of Co-O bonds at sites CoN_4 (left) and IrCoN_5 (right). Reprinted with permission from Ref. [81]. Copyright 2021 American Chemical Society.

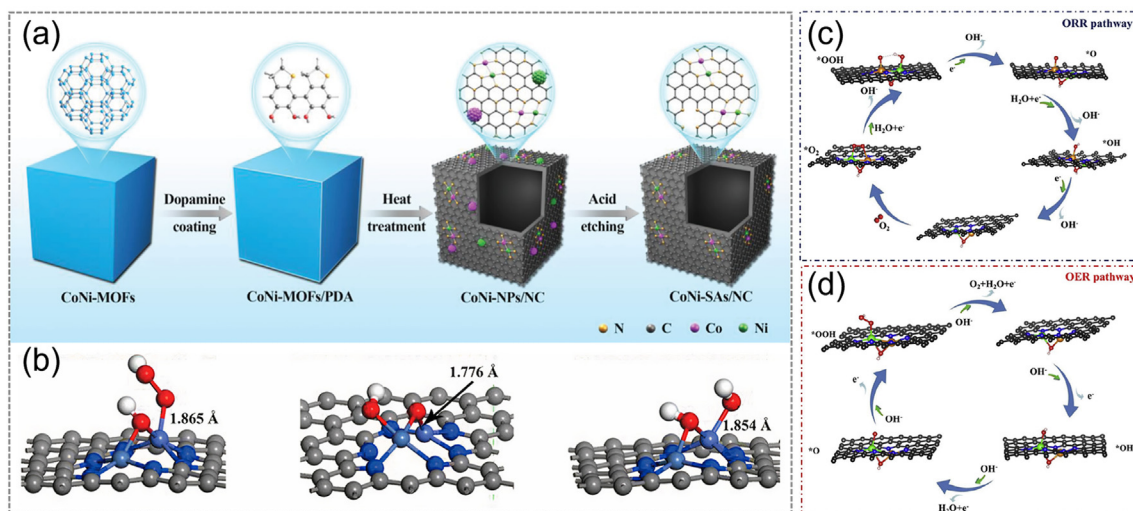


Fig. 7. Synergistic and bifunctional effect of heteronuclear bonded DACs as bifunctional electrocatalysts. (a) Schematic diagram of the synthesis process of CoNi-SAs/NC. (b) Optimized atomic configurations of oxygen intermediates on the Co-Ni-N model. Reprinted with permission from Ref. [84]. Copyright 2019 John Wiley & Sons. Proposed catalytic mechanisms of Fe-NiNC for (c) ORR and (d) OER. Black, blue, green, golden, red, and pink balls correspond to C, N, Ni, Fe, O, and H atoms, respectively. Reprinted with permission from Ref. [86]. Copyright 2020 Elsevier.

adsorption sites for reactant intermediates. This unique configuration facilitates the creation of novel coordination environments, which in turn optimizes the binding energies of the oxygen intermediates. Consequently, these DACs exhibit exceptional performance as bifunctional oxygen catalysts [52,79]. Based on the classification of existing catalysts, their mechanisms for enhancing bifunctional activity can be summarized into three main types. The first type involves the introduction of secondary metal species that can modulate the primary catalytic center, providing distinct absorption formations of different intermediates, and

ultimately improving overall activity. For example, Ma et al. synthesized a Ni₆₆Fe₃₄-NC sample with abundant presence of N₃-Fe-Ni-N₃ moieties (Fig. 6a) [80]. DFT simulations revealed that the Fe site in Ni(N₃)(OH)-Fe(N₃) possesses moderate adsorption properties for O-containing intermediates and serves as the primary active site for both ORR and OER. The neighboring Ni site, coordinated with OH, acts as an excellent mediator, adjusting the properties of the Fe site for efficient formation, association, and dissociation of OOH[•], thereby accelerating catalytic kinetics (Fig. 6b). A similar modulation effect can be observed in

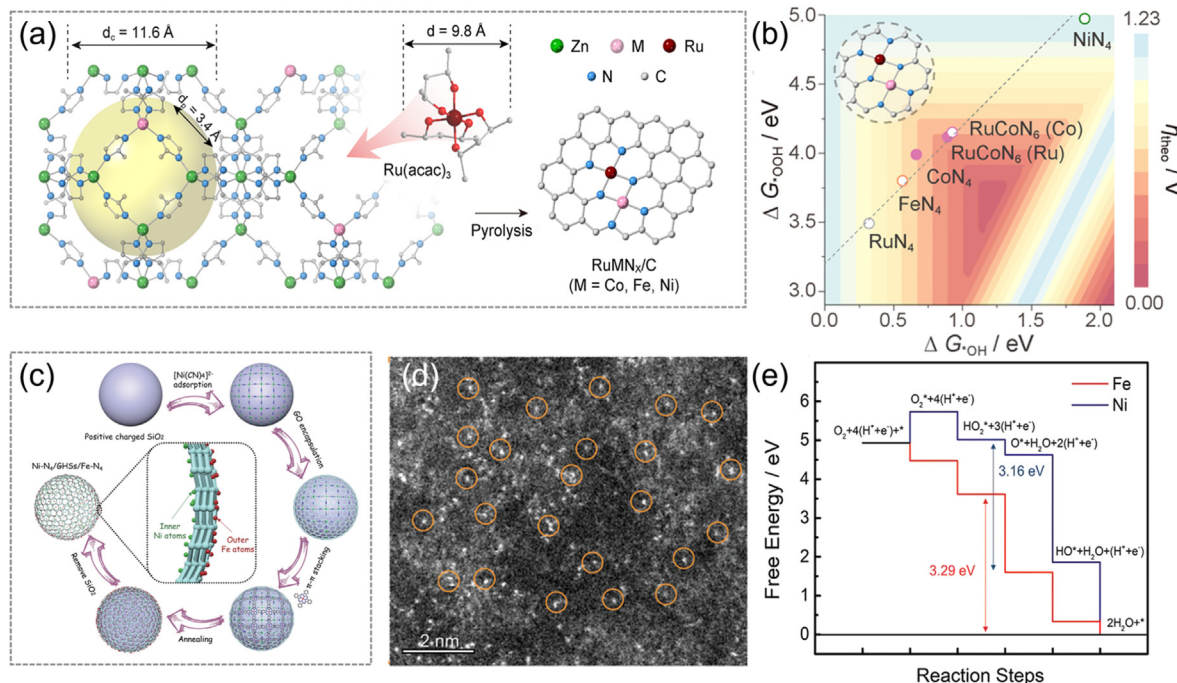


Fig. 8. Bridged DACs as bifunctional electrocatalysts. (a) Schematic diagram of RuMN_x/C synthesis strategy. d_c, d_p, and d represent the diameter of the cavity (ZIF-8), aperture (ZIF-8), and Ru (acac)₃ molecule, respectively. (b) Two-dimensional activity diagram ($U = 0$ V vs RHE) with the Gibbs free energies of ${}^{\bullet}\text{OH}$ ($\Delta G_{\bullet\text{OH}}$) and ${}^{\bullet}\text{OOH}$ ($\Delta G_{\bullet\text{OOH}}$) as first and second descriptors, respectively. The dashed line represents the linear proportional relationship between $\Delta G_{\bullet\text{OOH}}$ and $\Delta G_{\bullet\text{OH}}$. Reprinted with permission from Ref. [93]. Copyright 2022 American Chemical Society. Non-bonded DACs as bifunctional electrocatalysts. (c) Synthetic process of the Ni-N₄/GHSs/Fe-N₄ catalyst. (d) AC HAADF-STEM image of Ni-N₄/GHSs/Fe-N₄. (e) DFT calculated reaction free energies of oxygen electrocatalytic reactions ($U = 0$ V). Reprinted with permission from Ref. [101]. Copyright 2020 John Wiley & Sons.

combinations of noble and non-noble metals. In Chen et al.'s work, IrCo–N–C was prepared using a bimetallic organic framework encapsulation strategy (Fig. 6c) [81]. EXAFS fitting curves revealed a diatomic Ir–Co configuration contribution with a bond length of 2.30 Å, and the EXAFS-wavelet transform (WT) analysis further confirmed this structure (Fig. 6d). In this work, they discovered that the Co *d*-orbital electron configuration could be modulated by the introduced noble metal Ir single atom, thereby enhancing bifunctional activity. Theoretical calculations suggested that the Co site in an Ir–Co pair acts as the dominant active site for both ORR and OER catalysis. Meanwhile, the Ir site functions as an electronic modifier, inducing stronger spin polarization of the Co site, strengthening the Co–O binding affinity, and accelerating oxygen electrocatalysis (Fig. 6e and f).

In addition to the modulation effect, the synergistic effect of metal–metal atomic pairs can also be achieved [82,83]. For instance, Han et al. successfully synthesized Co–Ni DACs through the carbonization of dopamine-coated MOFs (Fig. 7a) [84]. The EXAFS spectra clearly indicated the presence of Co–N, Ni–N, and Co–Ni coordination. According to DFT simulations, the oxygen intermediate could be co-adsorbed by the Co–Ni pair, leading to reduced reaction energy barrier of the ORR and OER, thereby significantly enhancing the electrocatalytic activity (Fig. 7b). Zhang et al. further demonstrated that this synergistic effect can overcome the scaling factor and substantially improve bifunctional activity [85]. Moreover, the introduction of metal pairs could inhibit the competing two-electron-transfer reaction, thereby facilitating the four-electron-transfer ORR. These findings suggest that the synergistic interaction in heteronuclear bonded DACs endows them with considerable potential as bifunctional catalysts.

Moreover, the distinct metal active sites in heteronuclear bonded DACs can independently catalyze the ORR and OER, thereby achieving bifunctional electrocatalytic performance. For instance, Zhu et al. synthesized Fe–NiNC using the dual-solvent ion deposition method [86]. The presence of Ni–Fe moieties was confirmed by XANES. DFT calculations were used to investigate the origin of the bifunctional activity of Fe–NiNC. As depicted in Fig. 7c, during the ORR process, O₂ was initially adsorbed on the Ni–Fe bridge. When the O–O bond was broken, O adsorbed on the Fe atom at a lower formation energy. Subsequently, O* continuously reacted with H₂O to form *OH, and finally OH[−], to complete the ORR cycle. During the OER process, all intermediates were adsorbed on Ni sites, which were more active for OER (Fig. 7d).

4.2. Bridged DACs

Apart from bonded DACs, dual-atom sites with non-metal atoms (such as oxygen [87], nitrogen [88], and sulfur [89]) as bridges represent another type of DACs, which significantly increase the diversity of coordination structures. The bridging non-metal atom can redistribute electron densities between the dual single-metal sites in the bridged DACs, altering the charge state of the metals and thereby enhancing catalytic performance [90,91]. In addition, the theoretical calculation results showed that this structure is conducive to weakening the O=O bonds and had a high selectivity toward four-electron ORR pathway [92]. For example, Liu et al. employed a zeolithic imidazolate frameworks-8 (ZIF-8) template in a “precursor encapsulation–node substitution” strategy to synthesize RuM_N/C (M = Co, Fe, and Ni) DACs (Fig. 8a) [93]. Among these, RuCoN_x/C exhibited exceptional ORR/OER activity with a

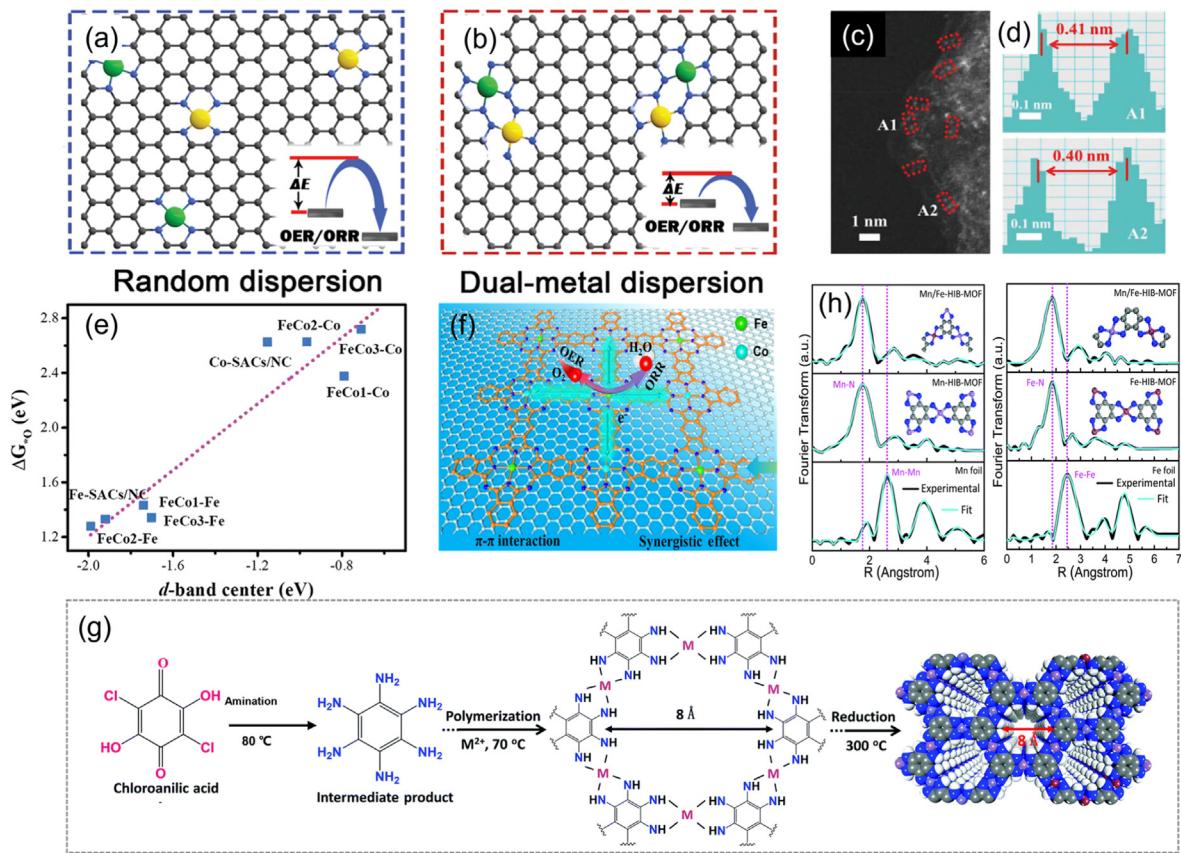


Fig. 9. Non-bonded DACs as bifunctional electrocatalysts. (a, b) Schematic diagram of the synthesis of different dispersion for FeCo-DACs/NC. AC HAADF-STEM image of FeCo-DACs/NC (c) and intensity profiles obtained for two metals (d). (e) The correlation between *d*-band center and energy ΔG_0 . Reprinted with permission from Ref. [105]. Copyright 2022 John Wiley & Sons. (f) Schematic diagram of the synthesis of PPcFeCo/3D-G. Reprinted with permission from Ref. [106]. Copyright 2023 Elsevier. (g) Synthesis schematic diagram of Mn/Fe-HIB-MOF. (h) Fourier-transform EXAFS spectra of different catalysts. Reprinted with permission from Ref. [107]. Copyright 2019 Royal Society of Chemistry.

low ΔE of 0.603 V. XANES and EXAFS results indicated that the two metals in RuCoN_x/C were coordinated in Ru–N₃ and Co–N₃ environment within a RuCoN₆ structure. Theoretical calculations further revealed that the combination of the *d*-block metal Co, with its electron-donating properties, can adjust the electronic state of the Ru atom, thereby balancing its strong adsorption properties for reactants in ORR (Fig. 8b). Bridged DACs exhibit modulation [94], synergistic [95–97], and bifunctional effects [91,98] in promoting bifunctional activity, similar to bonded DACs. Different coordination structures can lead to the electronic redistribution of metal active sites and consequently produce different reaction mechanisms [99]. For example, Zhang et al. proposed a dual-site cascade mechanism on the Fe/Mn–N_x–C catalysts during the ORR process [100]. DFT calculations revealed that the first three steps of ORR preferentially occur on the Fe-N_x sites due to the generated *OOH, *O, and *OH intermediates. Subsequently, *OH was transferred to adjacent Mn-N_x sites to complete the ORR process. It is worth noting that such synergistic cascade mechanisms may significantly influence reactions with multiple intermediates and should be considered in catalyst design.

4.3. Non-bonded DACs

The third category is non-bonded DACs, which consist of two distinct single-atom metals that do not bond with each other. Through precise chemical modulation, the spatial arrangement and distribution of isolated single-atom sites in the catalyst can show random or ordered distribution,

which enables various challenging catalytic reactions to proceed smoothly [102,103]. For example, Li et al. found that non-bonded DACs can adjust the adsorption configuration of ORR and improve catalytic performance due to long-range interactions between different active sites [104]. In addition, the absence of bonding between different metal sites introduces a wider range of structural possibilities. For instance, Ma and his colleagues incorporated Fe(II) phthalocyanine (FePc) into the surface of a NiN₄ precursor (SiO₂@[Ni(CN)₄]₂–@GO) via π - π stacking, subsequently obtaining non-bonded dual single-atom sites (Ni-N₄ and Fe-N₄) doped graphene hollow nanospheres (Ni-N₄/GHSs/Fe-N₄) through calcination and etching (Fig. 8c) [101]. The AC HAADF-STEM and EXAFS spectral results confirmed the presence of single-atom Ni and Fe species on the graphene (Fig. 8d). The unique Janus hollow graphene structure allowed for the deposition of Fe single atoms on the outer surface and Ni single atom sites on the inner surface, facilitating their respective functions as active sites of ORR and OER reactions, respectively, which avoids the competition of active sites on the same catalyst surface, thereby achieving superior bifunctional activity (Fig. 8e). Finally, the Ni-N₄/GHSs/Fe-N₄ exhibited a small ΔE of 0.790 V, demonstrating that non-bonded DACs can achieve spatial structural diversity of active sites for efficient bifunctional catalytic activity.

With further research, it has become increasingly apparent that the separation distance between two individual single atom sites in non-bonded DACs significantly influences catalyst performance. Molecular catalysts, characterized by their well-designed and flexible active centers,

Table 3
Bifunctional performance comparison of DACs in liquid-state ZABs.

Configuration	Catalyst	E (V vs. RHE)			Liquid-state ZABs				Ref.
		$E_{1/2}$	E_{10}	ΔE	OCV (V)	Peak power density (mW/cm ²)	Specific capacity (mAh/g _{Zn}) at current density (mA/cm ²)	Stability (h) at current density (mA/cm ²)	
Bonded	Fe ₂ /Co ₁ -GNCL	0.846	1.58	0.734	1.527	218	–	–	[76]
	Co ₂ -N-HCS-900	0.86	1.563	0.703	1.45	188.2	754.2@10	800@5	58.1 [116]
	IrCo-N-C	0.911	1.56	0.649	1.46	138.8	–	225@5	62.1 [81]
	Fe ₁ Co ₃ -NC-1100	0.877	1.579	0.702	1.479	372	–	190@10	– [82]
	Co ₁ Fe ₁ -N-C	0.933	1.67	0.677	–	227.7	782.4@20	230@2	68 [112]
	Fe,Co/DSA-NSC	0.879	1.44	0.561	1.52	240	748@10	60@10	– [113]
	Ni ₆₆ Fe ₃₄ -NC	0.849	1.697	0.848	1.44	140.1	765.5@10	334@20	– [80]
	FeNi-NPC HT	0.859	1.551	0.692	1.48	226.5	661@20	150@3 100@10	66.3 [83]
	Fe-NiNC-50	0.85	1.58	0.73	1.41	220	752.14@5	100@2	56.1 [86]
	FeNi SAs/NC	0.84	1.50	0.654	1.45	42.22	779.4@5	45@1	– [117]
	CoNi-SAs/NC	0.76	1.57	0.81	1.45	101.4	750.9@20	31@5	59.4 [84]
Bridged	Ni-SAs/HCNFs/Co-NAs	0.89	1.544	0.654	1.45	140.7	806.8@100	200@10	– [118]
	Fe/Co-N/S _{1.9} -C	0.836	1.524	0.688	1.52	138	763.2@20	16.66@10	– [89]
	CoFe-N-C	0.897	1.59	0.69	1.494	142.1	917.4@20	200@5	– [97]
	Fe ₁ Co ₁ -CNF	0.87	1.73	0.86	1.45	201.7	814@10	200@20	– [119]
	NiFe-CNG	0.82	1.5	0.68	–	185.9	–	–	– [87]
	Fe/Ni(1:3)-NG	0.842	1.71	0.868	1.50	164.1	824.3@5	120@5	– [98]
	Fe,Mn/N-C	0.928	1.62	0.692	1.4	160.8	902@5	81@5	– [94]
	FeCu-NC	–	–	0.63	1.492	231	–	300@5	58 [114]
	RuFe-N-C	0.92	1.55	0.63	1.52	139.9	916.1@20	200@5	– [88]
	IrFe-N-C	0.92	1.58	0.66	1.5	113.9	–	30@5	– [91]
	RuCoN _x /C	0.895	1.498	0.603	–	130	–	70@2	– [93]
Non-bonded	Ni-N ₄ /GHSs/Fe-N ₄	0.83	1.62	0.79	1.45	–	777.6@5	200@10	52.2 [101]
	FeCo-DACs/NC	0.877	1.6	0.723	1.5	175	–	240@10	– [105]
	PPcFeCo/3D-G	0.89	1.58	0.7	1.35	222	792@10	120@10	– [106]
	FeCo-NS-HNCs	0.87	1.525	0.655	1.48	168.0	846.5@10	250@5	60 [120]
	Fe,Co-SA/CS	0.86	1.59	0.73	1.43	86.65	819.6@5	100@5	– [121]
	Fe,Co,N-C	0.90	1.64	0.74	1.40	198.4	726@2	51@5	57.14 [102]
	Fe/CoN _x -C	0.85	1.56	0.71	1.52	134.97	798.25@10	80@10	51.48 [122]
	Mn/Fe-HIB-MOF	0.883	1.51	0.627	1.50	195	769@5	1000@10	62.33 [107]
	FeN ₄ -SC-NiN ₄	0.844	1.476	0.632	–	–	–	67@5	– [123]
	Fe, Ni-SAs/DNSC	0.93	1.58	0.65	–	160	802.5@10	32@10	– [124]
	FeNi-SAs@NC	0.907	1.528	0.621	1.54	260	950@5	140@5	– [125]
	Cu-Co/NC	0.92	1.565	0.645	1.45	295.9	752.2@20	510@10	60.1 [115]
	Ni ₁ Co ₁ -CNF	0.749	1.667	0.918	1.49	95.7	530@10	500@5	– [126]
	Co ₁ -PNC/Ni ₁ -PCN	0.88	1.62	0.74	1.59	252	874@100	45@10	– [127]

have recently been utilized to design catalysts with uniformly distributed diatomic sites. For instance, Bu et al. proposed a “pre-constrained metal twins” strategy to create FeCo-DACs/NC DACs containing adjacent FeN₄ and CoN₄ moieties in a homogeneous geometric configuration (Fig. 9b) [105]. The atomic distribution of Fe and Co atoms was confirmed by AC HAADF-STEM and EXAFS spectral results (Fig. 9c and d). Compared with the randomly dispersed FeN₄/CoN₄ moiety obtained by traditional methods (Fig. 9a), catalysts with a uniform geometric structure could optimize the *d*-band center position of the metal sites through electronic correlation between Fe and Co, thereby optimizing the free energy of the *O intermediate and resulting in improved catalytic activity (Fig. 9e). Similarly, Wang et al. successfully synthesized conjugated polymerized iron-cobalt phthalocyanine (PPcFeCo) by solid-state method, which was subsequently mixed with three-dimensional graphene (3D-G, Fig. 9f) [106]. The resulting PPcFeCo/3D-G DACs exhibited excellent bifunctional activity, which is attributed to the structural stability and uniform atomic anchoring of metal atoms provided by PPcFeCo. Lee and co-workers synthesized a novel three-dimensional dual-linked hex-aminobenzene MOF (Mn/Fe-HIB-MOF)-based oxygen electrocatalyst, which demonstrated a positive $E_{1/2}$ of 0.883 V for ORR and a low overpotential of 280 mV for OER (Fig. 9g) [107]. Fourier-transformed (FT)-EXAFS spectra verified the successful formation of the conjugated systems in Mn/Fe-HIB-MOF (Fig. 9h). Furthermore, DFT calculations indicated that the well-defined planar structure of Mn/Fe-HIB-MOF (non-deformation along the basal plane) contributed to enhanced bifunctional activity. These examples illustrate that the strategic construction of diatomic sites in molecular catalysts and the design of catalyst structures with uniformly distributed active sites are advantageous for improving the bifunctional properties of the catalyst. However, our current understanding of the relationship between the atomic distance between diatomic sites and the performance in non-bonded DACs is not yet well-defined. When two metal atoms are in close proximity, they interact not only spatially but also electronically, facilitating intricate catalytic reactions [108,109]. Nevertheless, existing characterization methods primarily provide an average representation of active site parameters in catalysts, making it challenging to precisely define the

distance between dual atoms and establish an accurate structure-property relationship [110,111]. Therefore, further comprehensive exploration and research are necessary in order to address this gap.

In this section, we discuss DACs with different structure characteristics, highlighting how homonuclear bonded DACs can augment catalytic activity by optimizing the adsorption of reactants or key intermediates. In heteronuclear DACs, two distinct single-atom metals can be metal-bonded, bridged, or exist in isolated structures, thereby promoting catalytic reactions through modulation, synergistic, and bifunctional effects. Moreover, molecular catalysts with dual atom sites offer greater flexibility in the construction of active sites.

5. Applications of DACs in ZABs

Based on the excellent structural characteristics of DACs mentioned previously, in this section, we will discuss their practical performance as bifunctional catalysts in liquid and solid-state ZABs.

5.1. Applications in liquid-state ZABs

Table 3 presents a comprehensive overview of the performance of DACs in liquid-state ZABs in recent years. With the advancement of liquid-state ZABs and the unique structural advantages offered by DACs as bifunctional catalysts, this section focuses on the remarkable achievements of three types of DACs: bonded, bridged, and non-bonded DACs. Xu and his coworkers synthesized dual-atom CoFe-N-C nanorods (Co₁Fe₁-N-C NRs) using a ZIF-derived strategy followed by thermal fixation treatment [112]. The CoFe-N-C bonded DAC exhibited excellent ORR activity and stability, enabling stable charge/discharge cycles in liquid-state ZABs. The author also conducted theoretical calculations, revealing that the adjacent Co–Fe diatomic sites acted synergistically as unique adsorption sites, endowing CoFe-N-C with the potential for iodine oxidation. By incorporating potassium iodide (KI) additive into the assembled liquid-state ZAB, it achieved a charge voltage as low as 1.76V and demonstrated ultra-long cycle stability of over 230 h,

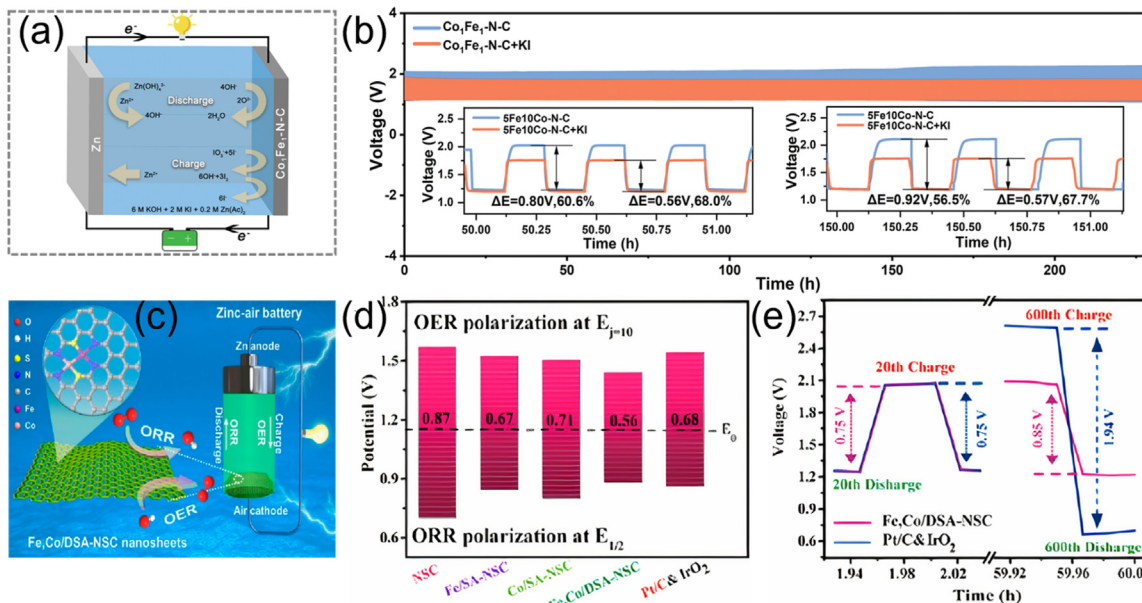


Fig. 10. Bonded DACs as bifunctional electrocatalysts for liquid-state ZABs. (a) Schematic diagram of liquid-state ZABs containing KI additive. (b) Cyclic stability of the battery at 2 mA/cm². Reprinted with permission from Ref. [112]. Copyright 2023 John Wiley & Sons. (c) Schematic illustration of Fe,Co/DSA-NSC as a bifunctional catalyst for liquid-state ZABs. (d) ΔE of different catalysts. (e) Bloated cycling potential gap at 10 mA/cm². Reprinted with permission from Ref. [113]. Copyright 2023 American Chemical Society.

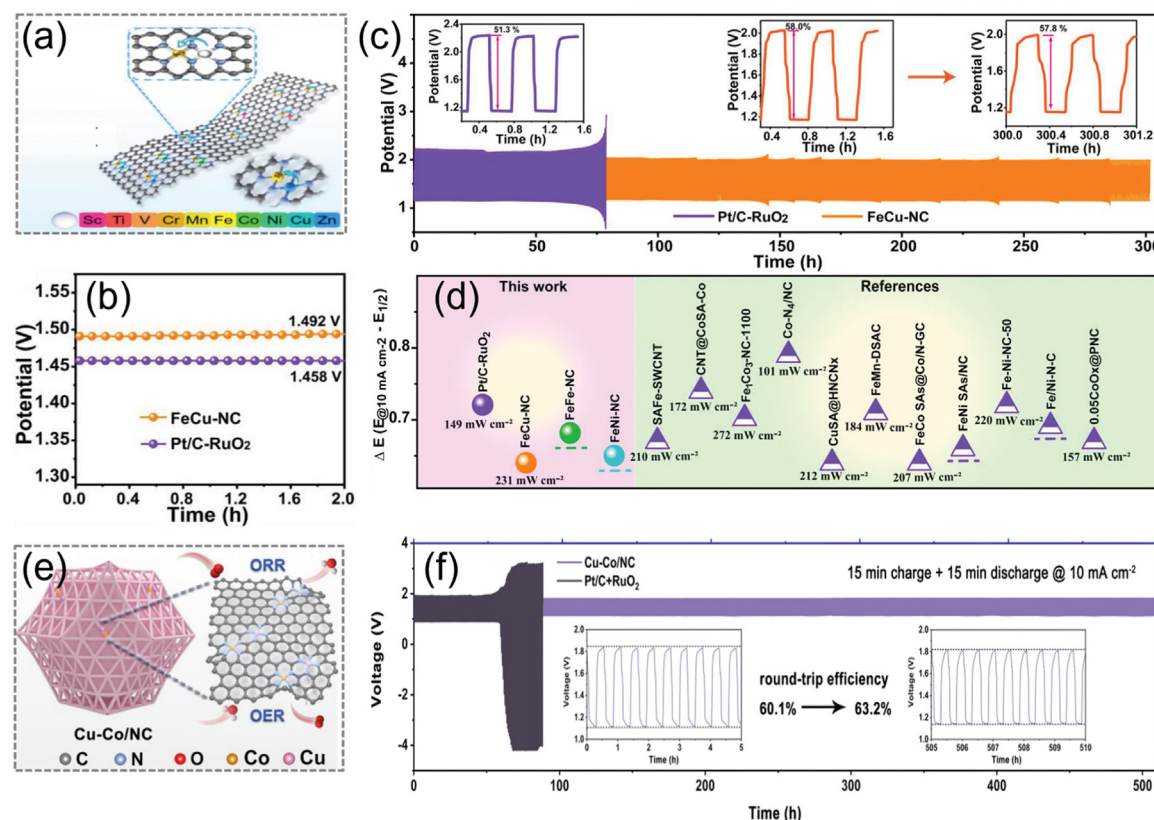


Fig. 11. (a) Schematic illustration of synthesizing DACs. (b) OCVs of different catalysts. (c) Charge/discharge stabilities at the current density of 5.0 mA/cm². (d) Comparison of ΔE of different catalysts and peak power density of corresponding assembled liquid-state ZABs. Reprinted with permission from Ref. [114]. Copyright 2023 John Wiley & Sons. (e) Schematic illustration of Cu-Co/N/C as a bifunctional catalyst. (f) Cyclic stability of the battery at 10 mA/cm². Reprinted with permission from Ref. [115]. Copyright 2023 John Wiley & Sons.

significantly enhancing energy efficiency (Fig. 10a and b). Additionally, Zhao et al. developed an atomic-interfacial-regulation method to fabricate a FeCo-bonded DAC (Fe,Co/DSA-NSC, Fig. 10c) [113]. The Fe/Co dual atomic sites, characterized by an asymmetric arrangement of N and S coordination, effectively facilitated charge transfer, reduced the energy barrier of oxygenated reaction intermediates, and enhanced reaction kinetics. Thus, Fe,Co/DSA-NSC exhibited excellent bifunctional activity, with a remarkably low ΔE of 0.56V (Fig. 10d). Experimental results from continuous charge/discharge cycles over 60 h demonstrated negligible changes in the voltage gaps of the Fe,Co/DSA-NSC-based battery, highlighting its commendable robustness (Fig. 10e).

Furthermore, bridged DACs and non-bonded DACs also show strong potential for applications in liquid-state ZABs. For instance, Li et al. utilized DFT calculations to compare DACs composed of late transition metals (Mn, Co, Ni, Cu, and Zn) with Fe to those containing early transition metals (Sc, Ti, V, and Cr, Fig. 11a) [114]. The former exhibited more effective optimization of ORR and OER by lowering the adsorption-free energy at Fe sites. Practical experiments confirmed that FeCu-NC bridged DAC exhibited superior bifunctional properties, achieving a remarkably low ΔE of 0.63V. Assembled liquid-state ZABs based on this catalyst delivered a high OCV of 1.492V, a high peak power density of up to 231 mW/cm² and demonstrated stable charge/discharge performance for over 300 h at a current density of 5.0 mA/cm² (Fig. 11b and d). Li et al. synthesized a non-bonded DAC by dispersing Cu-Co diatomic sites on a high-porosity nitrogen-doped carbon support (Cu-Co/NC, Fig. 11e) [115]. Theoretical calculations indicated that the synergistic effect between the bimetallic sites, characterized by a metal-N₄ coordination structure, induced asymmetric charge distribution and facilitated optimal adsorption/desorption behavior of oxygen intermediates. Liquid-state ZABs assembled using Cu-Co/NC as cathode

material achieved a maximum peak power density of 231 mW/cm² and demonstrated stable charge/discharge performance for over 300 h at a current density of 5.0 mA/cm² (Fig. 11f).

5.2. Applications in solid-state ZABs

In recent years, there has been a growing interest in the applications of flexible devices in wearable and portable electronic devices, leading to the development for solid-state ZABs. The key difference between solid-state ZABs and liquid-state ZABs lies in the use of (semi)-solid electrolytes. Currently, gel polymers such as polyacrylamide (PAM), polyacrylic acid (PAA), polyvinyl alcohol (PVA), and sodium polyacrylate (PANa) hydrogel are commonly employed as electrolytes [128]. Among these, PAM-based electrolytes have demonstrated superior robustness and adaptability to a wide temperature range [129–133]. However, solid-state ZABs face challenges such as sluggish kinetics for ORR/OER and limited oxygen diffusion properties in (semi)-solid electrolytes, highlight the need of bifunctional catalysts with improved activity. To address these challenges, researchers have focused on the application of DACs for solid-state ZABs, which were inspired by the excellent performance of DACs in liquid-state ZABs. Table 4 provides a detailed summary of the performance of various DACs as bifunctional oxygen electrocatalysts in solid-state ZABs.

Among the studies conducted, notable progress has been achieved by designing bifunctional oxygen electrocatalysts with unique structural features. For example, Deng et al. developed a bio-cooperative process to design FeNi diatomic sites on N and P co-doped carbon hollow tyre, resulting in the formation of FeNi-NPC HT (Fig. 12a) [83]. This unique combination of Fe-Ni dual centers and N, P heteroatoms synergistically enhanced the ORR/OER activity. The highly porous carbon structure

Table 4
Bifunctional performance comparison of DACs in solid-state ZABs.

Configuration	Catalyst	E (V vs. RHE)			Solid-state ZABs					Ref.	
		$E_{1/2}$	$E_{j=10}$	ΔE (V)	OCV (V)	Peak power density (mW/cm ²)	Specific capacity (mAh/g _{Zn}) at current density (mA/cm ²)	Stability (h) at current density (mA/cm ²)	Round-trip efficiency (%)		
12	Bonded	Fe-Se/NC ^{a)}	0.925	1.623	0.698	1.47 (25 °C) 1.44 (-40 °C)	135 (25 °C) 71 (-40 °C)	764@5 (25 °C) 697@1 (-40 °C)	200@20 (25 °C) 741@1 (-40 °C) 133@5 (-40 °C)	68.51	PAM [138]
		Fe ₁ Co ₁ -CNF	0.87	1.73	0.86	—	—	—	3@2	—	PVA [119]
		Fe ₁ Co ₃ -NC-1100	0.877	1.579	0.702	—	—	—	6@10	—	PAA [82]
		NCAG/Fe-Co	0.89	1.523	0.633	1.47	117	—	1000 cycles@5	—	PAM [140]
		FeNi-NPC HT	0.859	1.551	0.692	—	—	—	100 cycles@4	—	PAA [83]
		CoNi-SAs/NC	0.76	1.57	0.81	—	—	—	6.66@1	—	PVA [84]
		Ni-SAs/HCNFs/Co-NAs	0.89	1.544	0.654	1.38	57.6	—	82@10	59.4	PVA [118]
		FeMn-DSAC	0.922	1.635	0.713	1.45 (25 °C) 1.44 (-40 °C)	184 (25 °C) 30 (-40 °C)	734@2 (25 °C) 631@2 (-40 °C)	80@2 (25 °C) 29@2 (-40 °C)	63.21	PAM [95]
		Fe,Mn/N-C	0.928	1.62	0.692	1.333	—	—	6@1	—	PVA [94]
		Fe/Ni-N-C	0.861	1.552	0.691	—	—	—	10@5	—	PVA [96]
12	Bridged	FeCo-DACs/NC	0.877	1.6	0.723	1.466	—	—	28@10	—	PAA [105]
		FeCo-NS-HNCs	0.87	1.525	0.655	1.439	206.4	1123@10	30@1	60	— [120]
		Fe ₃ Co ₇ -NC	0.893	1.573	0.68	1.51	133 (30 °C) 34 (-30 °C) 156 (60 °C)	747@2	400@2 (30 °C) 666@2 (-30 °C) 110@2 (60 °C)	62.89	PAA [139]
		Fe ₂ Co ₃ N-C	0.90	1.64	0.74	1.33	158	—	34@2	67.4	PVA [102]
		Fe/CoN _x -C	0.85	1.56	0.71	1.51	62.16	—	43.33@1	51.48	PAA [122]
		FeNi-SAs@NC	0.907	1.528	0.621	1.23	70	—	13@1	—	PVA [125]
		NCAG/Fe-Cu	0.94	1.61	0.67	1.51	186	—	800 cycles@5	57	PANa [141]
		Mn/Fe-HIB-MOF	0.883	1.51	0.627	1.442	194	750@5	600@25	65.24	Bio-cellulose nanofibrous [107]
		PPcFeCo/3D-G	0.89	1.58	0.7	—	59	—	25@5	—	PVA [106]
		Ni ₁ Co ₁ -CNF	0.749	1.667	0.918	—	—	—	6.66@1	—	PVA [126]

Note: Except for special mark, all solid-state ZABs are sandwich-type and operate at room temperature. ^{a)} Represents cable-type solid-state ZAB.

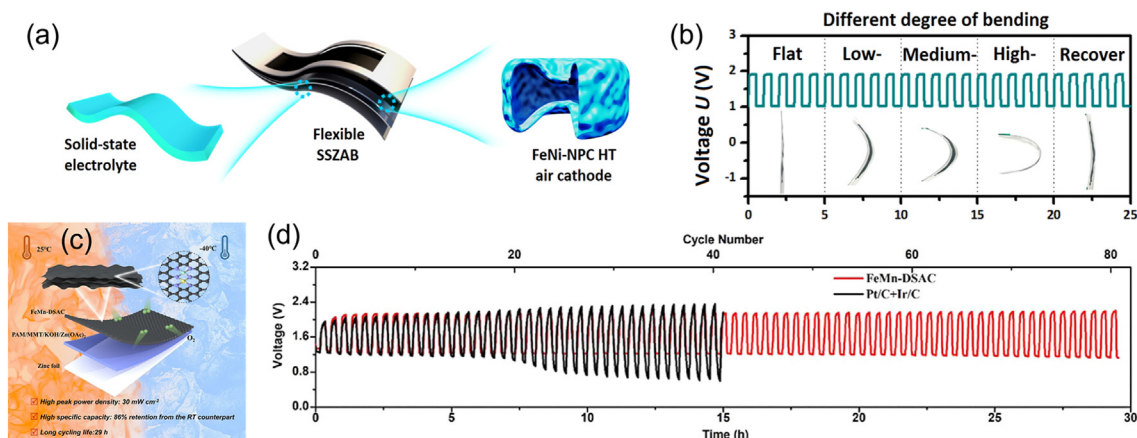


Fig. 12. (a) Sandwich-type ZABs based on FeNi-NPC HT as a cathode. (b) Galvanostatic charge/discharge profiles of the solid-state ZABs in different bending states. Reprinted with permission from Ref. [83]. Copyright 2023 Elsevier. (c) Schematic illustration of FeMn-DSAC as a bifunctional catalyst for solid-state ZABs. (d) Galvanostatic cycling stability at 2 mA/cm² of FeMn-DSAC and Pt/C + Ir/C as a bifunctional catalyst at -40 °C. Reprinted with permission from Ref. [95]. Copyright 2022 John Wiley & Sons.

with a hollow center not only generated a large number of active sites but also facilitated rapid kinetics in the operation of solid-state ZABs. Moreover, the FeNi-NPC HT-based batteries demonstrated stable charge/discharge curves under various bending states (Fig. 12b). Another

noteworthy study was conducted by Cui et al., who employed a molten salt-assisted pyrolysis strategy to prepare a novel bridged dual single-atom catalyst (FeMn-DSAC) [95]. Fe-N₄ and Mn-N₄ sites were constructed on 2D ultrathin N-doped carbon nanosheets with a porous

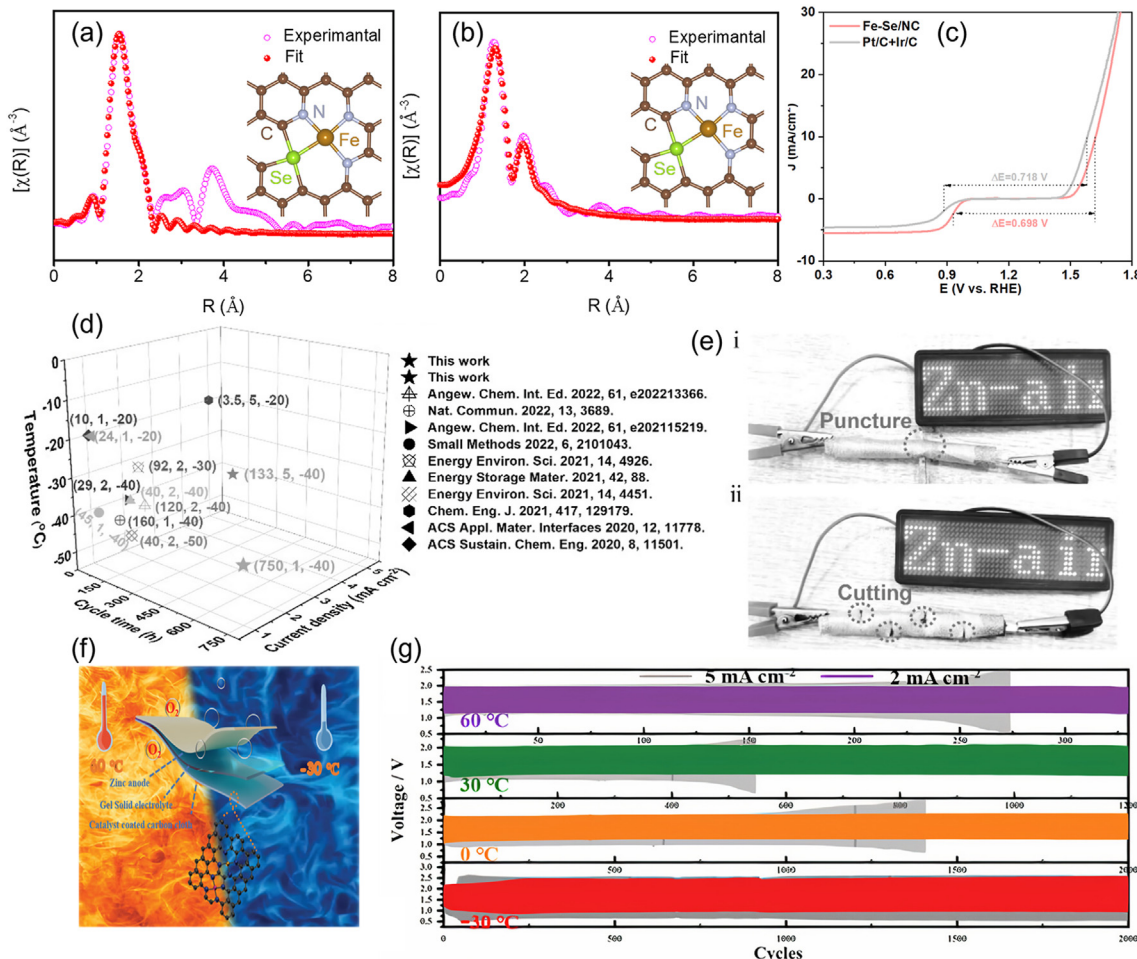


Fig. 13. Fourier-transform EXAFS spectra and fit in R space of Fe (a) and Se (b) in Fe-Se/NC. (c) Bifunctional polarization curves of Fe-Se/NC and Pt/C + Ir/C. (d) Comparison with reported low-temperature ZABs. (e) Optical images of LED screens powered by Fe-Se/NC-based battery under i-puncture and ii-cutting. Reprinted with permission from Ref. [138]. Copyright 2023 John Wiley & Sons. (f) Schematic illustration of Fe₃Co₇-NC as a bifunctional catalyst for solid-state ZABs. (g) Cycling tests of the Fe₃Co₇-NC at 2 and 5 mA/cm² and at different temperatures. Reprinted with permission from Ref. [139]. Copyright 2022 John Wiley & Sons.

structure (Fig. 12c). FeMn-DSAC exhibited remarkable bifunctional activity with a low ΔE of 0.713 V, which was attributed to the synergistic effect of Fe/Mn dual-sites facilitating $^{*}\text{OOH}$ dissociation and the porous 2D nanosheet structure. Notably, at a current density of 2 mA/cm^2 , FeMn-DSAC-based solid-state ZABs exhibited stable cycling for up to 30 h, twice as long as commercial catalysts (Fig. 12d).

With the diversity of human activities, such as polar inspection, aerospace, deep-sea exploration, etc., the development of solid-state ZABs that can operate under extreme conditions has attracted much attention in recent years. However, under extreme conditions, the slowdown of ORR/OER kinetics [134,135] and extremely high O=O bond energy [136,137] led to serious deterioration of the performance of ZABs. In this context, DACs also show potential for application in low-temperature solid-state ZABs. One notable example is the work of Wang et al., who synthesized a bifunctional electrocatalyst consisting of atomically dispersed Fe-Se atomic pairs supported on N-doped carbon (Fe-Se/NC) [138]. The EXAFS spectra confirmed the existence of Fe-Se bonds (Fig. 13a and b). Through experimental and theoretical studies, they discovered that the introduction of Se could regulate the electronic structure and micro-environment of the Fe sites through unconventional *p-d* orbital hybridization, thus optimizing the adsorption/desorption behavior during the ORR/OER processes. Fe-Se/NC exhibited a low ΔE of 0.698 V, far superior to that of reported Fe-based single-atom catalysts. (Fig. 13c). When assembling solid-state ZABs with a cable structure, utilizing a modified organohydrogel as the electrolyte resistant to temperatures as low as -40°C , Fe-Se/NC-based ZABs demonstrated superior cycling performance compared with previously reported low-temperature ZABs employing other types of catalysts. Moreover, when operated at current densities of 1 and 5 mA/cm^2 under -40°C , the battery exhibited impressive long-term stability, with continuous operation for up to 741 and 133 h, respectively (Fig. 13d). Furthermore, an intriguing observation was made regarding the performance of a light-emitting diode (LED) powered by this battery. Despite being subjected to puncturing or cutting, the LED remained functional, underscoring the robustness and reliability of Fe-Se/NC bonded DAC (Fig. 13e). In another study, Cu et al. synthesized a non-bonded DAC featuring isolated Fe and Co dual sites, which was guided by first-principles calculations (Fig. 13f) [139]. The presence of Fe-Co bimetal promoted oxygen binding with low activation energy, promoting ORR, while the formation of the Fe-O-O-Co bond served as a crucial intermediate for OER. These characteristics endowed $\text{Fe}_3\text{Co}_7\text{-NC}$ with excellent ORR/OER properties. Upon integration into the sandwich-type ZABs, $\text{Fe}_3\text{Co}_7\text{-NC}$ -based ZABs exhibited excellent cycling performance. They could be cycled at 2 mA/cm^2 for over 2000 cycles at low-temperature (-30°C) and over 340 cycles at high-temperature (60°C) without obvious fading in the operating voltage (Fig. 13g). These results highlight the robust cycling stability of $\text{Fe}_3\text{Co}_7\text{-NC}$ -based ZABs, underscoring their potential as reliable and flexible energy storage devices that adapt well across a wide temperature range.

In conclusion, this section has summarized the applications of different types of DACs as bifunctional catalysts in liquid and solid-state ZABs. The application of DACs has significantly improved the performance of liquid-state ZABs, especially the long-term cycling stability. In addition, DACs can also be applied to liquid-state ZABs modified with potassium iodide to further improve energy efficiency and service life. By applying DACs to solid-state ZABs (cable and sandwich-type), the battery can operate normally in harsh environments such as puncturing, cutting, bending, and low temperatures, demonstrating the strong adaptability of DACs.

6. Summary and perspectives

Rechargeable ZABs hold great promise to address contemporary energy and environmental challenges. However, the practical application of ZABs requires the development of efficient bifunctional oxygen electrocatalysts. In recent years, the utilization of DACs in ZABs has garnered

significant attention. This comprehensive review highlights the advantages of DACs with unique configurations (bonded, bridged, and non-bonded) as bifunctional catalysts. Furthermore, we provide a summary of the current applications of DACs in both liquid and solid-state ZABs. Despite notable progress, the research on DACs is still in its early stages, presenting both challenges and opportunities for further advancements.

- (1) Precise design and controlled synthesis of DACs. The controlled synthesis of DACs with specific configurations remains a significant challenge. Current methodologies, such as high-temperature pyrolysis, suffer from drawbacks such as unpredictable coordination configurations, metal site aggregation, and low metal loading. To overcome these limitations, alternative strategies need to be explored. For instance, the pyrolysis-free synthesis of catalysts derived from covalent organic frameworks/hydrogen-bonded organic frameworks offers well-defined active sites and controllable coordination environments, providing valuable insights for the future design and synthesis of DACs [142]. Further research is required to investigate the structure-performance relationship of different types of DACs. It is important to address the limitations of characterization methods and controllable synthesis in order to obtain a comprehensive understanding. Currently, many studies fail to acknowledge the simultaneous existence of multiple types of active sites within the same catalytic system [70,79]. This oversight can have a significant impact on the establishment of accurate structure-performance relationship. Therefore, it is crucial to establish a comprehensive structure-activity-mechanism relationship for different DAC structures, which can pave the way for the rational design and optimization of DACs for enhanced ORR/OER performance.
- (2) Identification of dynamic evolution of diatomic active sites. Catalytic reactions involve dynamic cyclic processes generating numerous intermediates, necessitating the identification of the dynamic evolution of active sites. Advanced in-situ characterization techniques are crucial to track these dynamic changes and guide the design and synthesis of next-generation catalysts. For example, in-situ/operando spectro-electrochemical techniques can be employed to detect the dynamic evolution of active sites, as demonstrated by Tong et al., who combined in-situ XANES and DFT to reveal the impact of evolved $\text{Mn}^{+3.8}\text{-N}_3\text{C}$ and $\text{Mn}^{+3.2}\text{-N}_2\text{C}_2$ structures on ORR activity [143].
- (3) Expanding and optimizing the combination of diverse elements and precisely regulating the diatomic coordination environment represent pivotal strategies for enhancing the bifunctional electrocatalytic performance of DACs. While the majority of DACs currently based on transition metal elements, the periodic table offers a plethora of unexplored possibilities. Notably, the rare earth elements, characterized by the occupation of their *4f* orbitals, have demonstrated remarkable potential [144,145]. Furthermore, meticulous control over the coordination environment of DACs presents an effective avenue for improving their bifunctional electrocatalytic performance. However, investigations targeting the modification of DACs pertaining to the first and second shells, as well as carbon support, remain relatively scarce, thus underscoring the expansive scope for future research endeavors [142].
- (4) Strengthening the guiding role of theoretical calculations in DAC research is of utmost importance. In addition to DFT, harnessing advanced tools such as machine learning is imperative for accurate predictions and effective guidance in experimental synthesis. Through comprehensive collection and analysis of existing databases, we can delve into the intricate reaction mechanisms and provide meticulous guidance for experimental design. Moreover, microkinetic models should be developed to study the kinetics of intermediate catalytic reactions. By employing such theoretical calculations, we can propel the advancement of DAC research,

- expedite the discovery and development of novel catalysts, and ultimately realize more efficient and sustainable energy conversion and storage technologies.
- (5) Enhancing cycling performance of ZABs. Improving the stability and longevity of ZABs during charge/discharge cycles, especially under high current densities, is pivotal for practical applications. Carbon-based catalysts suffer from carbon oxidation/corrosion at high OER potentials, limiting their stability. Therefore, strategies such as reinforcing the anchoring of diatomic active sites on corrosion-resistant carbon supports of DACs is a promising solution. Additionally, how to experimentally evaluate the intrinsic catalytic activity is in urgent need. Current experimental evaluation is usually mixed up with many extrinsic factors, such as the morphology and conductivity of the catalyst support, macro- and micro-environment of catalyst, pH values, and temperature, etc. These extrinsic factors can obscure the true intrinsic catalytic activity and hinder accurate assessments. To further enhance the cycle life of ZABs, it is also essential to comprehensively improve the performance of each key component, such as optimizing zinc electrodes. By focusing on the optimization of zinc electrodes, the overall performance of ZABs can be further enhanced, leading to improved cycle life and practical viability [146].

Declaration of competing interest

The authors declare that they have no known competing financial interests or personal relationships that could have appeared to influence the work reported in this paper.

Acknowledgements

This work was supported by the Research Grants Council of the Hong Kong Special Administrative Region, China (PDFS2223-5S03 and PDFS2122-5S02) and the Hong Kong Polytechnic University (YWA1, YWB6, ZE2F, CDBG, and WZ5L).

References

- [1] H. Sun, X. Xu, H. Kim, Z. Shao, W. Jung, Advanced electrocatalysts with unusual active sites for electrochemical water splitting, *InfoMat* (2023) e12494, <https://doi.org/10.1002/inf2.12494>.
- [2] G. Chen, C. Wei, Y. Zhu, H. Huang, Emerging chemical driving force in electrocatalytic water splitting, *EcoMat* 5 (2023) e12294, <https://doi.org/10.1002/eom2.12294>.
- [3] L. Li, G. Chen, Z. Shao, H. Huang, Progress on smart integrated systems of seawater purification and electrolysis, *Energy Environ. Sci.* 16 (2023) 4994–5002, <https://doi.org/10.1039/D3EE02712K>.
- [4] Y. Li, G. Chen, H.-C. Chen, Y. Zhu, L. Fei, L. Xu, T. Liu, J. Dai, H. Huang, W. Zhou, Tailoring the surface cation configuration of Ruddlesden-Popper perovskites for controllable water oxidation performance, *Energy Environ. Sci.* 16 (2023) 3331–3338, <https://doi.org/10.1039/D3EE00380A>.
- [5] X. Lin, Y. Hu, K. Hu, X. Lin, G. Xie, X. Liu, K.M. Reddy, H.-J. Qiu, Inhibited surface diffusion of high-Entropy Nano-Alloys for the preparation of 3D Nanoporous graphene with high Amounts of single atom Dopants, *ACS Mater. Lett.* 4 (2022) 978–986, <https://doi.org/10.1021/acsmaterialslett.2c00245>.
- [6] Y. Zhu, G. Chen, Y.-C. Chu, C.-S. Hsu, J. Wang, C.-W. Tung, H.M. Chen, Heteroatomic pairs with a distal Fe^{3+} -site Boost water oxidation, *Angew. Chem. Int. Ed. Engl.* 61 (2022) e202211142, <https://doi.org/10.1002/anie.202211142>.
- [7] P. Poizot, S. Laruelle, S. Gruegeon, L. Dupont, J. Tarascon, Nano-sized transition-metal oxides as negative-electrode materials for lithium-ion batteries, *Nature* 407 (2000) 496–499, <https://doi.org/10.1038/35035045>.
- [8] J. Cabana, L. Monconduit, D. Larcher, M.R. Palacin, Beyond intercalation-based Li-ion batteries: the state of the art and challenges of electrode materials reacting through conversion reactions, *Adv. Mater.* 22 (2010) E170–E192, <https://doi.org/10.1002/adma.201000717>.
- [9] M. Winter, B. Barnett, K. Xu, Before Li ion batteries, *Chem. Rev.* 118 (2018) 11433–11456, <https://doi.org/10.1021/acs.chemrev.8b00422>.
- [10] V. Etacheri, R. Marom, R. Elazari, G. Salitra, D. Aurbach, Challenges in the development of advanced Li-ion batteries: a review, *Energy Environ. Sci.* 4 (2011) 3243–3262, <https://doi.org/10.1039/C1EE01598B>.
- [11] X. Dong, L. Chen, X. Su, Y. Wang, Y. Xia, Flexible aqueous lithium-ion battery with high safety and large volumetric energy density, *Angew. Chem. Int. Ed. Engl.* 55 (2016) 7474–7477, <https://doi.org/10.1002/anie.201602766>.
- [12] Y. Yang, Y. Tang, G. Fang, L. Shan, J. Guo, W. Zhang, C. Wang, L. Wang, J. Zhou, S. Liang, Li^+ intercalated $\text{V}_2\text{O}_5\text{-NH}_2\text{O}$ with enlarged layer spacing and fast ion diffusion as an aqueous zinc-ion battery cathode, *Energy Environ. Sci.* 11 (2018) 3157–3162, <https://doi.org/10.1039/C8EE01651H>.
- [13] J. Fu, Z.P. Cano, M.G. Park, A. Yu, M. Fowler, Z. Chen, Electrically rechargeable zinc-air batteries: progress, challenges, and perspectives, *Adv. Mater.* 29 (2017) 1604685, <https://doi.org/10.1002/adma.201604685>.
- [14] Q. Liu, Z. Pan, E. Wang, L. An, G. Sun, Aqueous metal-air batteries: Fundamentals and applications, *Energy Stor. Mater.* 27 (2020) 478–505, <https://doi.org/10.1016/j.ensm.2019.12.011>.
- [15] J.S. Lee, S. Tai Kim, R. Cao, N.S. Choi, M. Liu, K.T. Lee, J. Cho, Metal-air batteries with high energy density: Li-air versus Zn-air, *Adv. Energy Mater.* 1 (2011) 34–50, <https://doi.org/10.1002/aenm.201000010>.
- [16] C. Xu, Y. Niu, V. Ka-Man Au, S. Gong, X. Liu, J. Wang, D. Wu, Z. Chen, Recent progress of self-supported air electrodes for flexible Zn-air batteries, *J. Energy Chem.* 89 (2024) 110–136, <https://doi.org/10.1016/j.jecchem.2023.10.038>.
- [17] X. Wang, L. Xu, C. Zhou, N.H. Wong, J. Sunarso, R. Ran, W. Zhou, Z. Shao, Toward self-supported bifunctional air electrodes for flexible solid-state Zn-air batteries, *Small Sci.* 3 (2023) 2300066, <https://doi.org/10.1002/smsc.202300066>.
- [18] A. Kundu, S. Mallik, S. Ghora, C.R. Raj, Advanced oxygen electrocatalyst for air-breathing electrode in Zn-air batteries, *ACS Appl. Mater. Interfaces* 13 (2021) 40172–40199, <https://doi.org/10.1021/acsami.1c08462>.
- [19] X. Xu, Y. Pan, Y. Zhong, C. Shi, D. Guan, L. Ge, Z. Hu, Y.Y. Chin, H.J. Lin, C.T. Chen, New Undisputed evidence and strategy for enhanced lattice-oxygen Participation of Perovskite electrocatalyst through cation Deficiency Manipulation, *Adv. Sci.* 9 (2022) 2200530, <https://doi.org/10.1002/advs.202200530>.
- [20] J. Li, H. Xue, N. Xu, X. Zhang, Y. Wang, R. He, H. Huang, J. Qiao, Co/Ni dual-metal embedded in heteroatom doped porous carbon core-shell bifunctional electrocatalyst for rechargeable Zn-air batteries, *Materials Reports: Energy* 2 (2022) 100090, <https://doi.org/10.1016/j.matre.2022.100090>.
- [21] B. Qiao, A. Wang, X. Yang, L.F. Allard, Z. Jiang, Y. Cui, J. Liu, J. Li, T. Zhang, Single-atom catalysis of CO oxidation using Pt_1/FeO_x , *Nat. Chem.* 3 (2011) 634–641, <https://doi.org/10.1038/nchem.1095>.
- [22] X. Zheng, B. Li, Q. Wang, D. Wang, Y. Li, Emerging low-nuclearity supported metal catalysts with atomic level precision for efficient heterogeneous catalysis, *Nano Res.* 15 (2022) 7806–7839, <https://doi.org/10.1007/s12274-022-4429-9>.
- [23] X. Lin, Q. Li, Y. Hu, Z. Jin, K.M. Reddy, K. Li, X. Lin, L. Ci, H.J. Qiu, Revealing atomic configuration and synergistic interaction of single-atom-based Zn-Co-Fe Trimetallic sites for enhancing oxygen reduction and evolution reactions, *Small* 19 (2023) 2300612, <https://doi.org/10.1002/smll.202300612>.
- [24] J. Gao, X. Zhou, Y. Wang, Y. Chen, Z. Xu, Y. Qiu, Q. Yuan, X. Lin, H.J. Qiu, Exploiting the synergistic electronic interaction between Pt-Skin Wrapped Intermetallic PtCo nanoparticles and Co-N-C support for efficient ORR/EOR electrocatalysis in a direct Ethanol fuel Cell, *Small* 18 (2022) 2202071, <https://doi.org/10.1002/smll.202300612>.
- [25] X.-F. Yang, A. Wang, B. Qiao, J. Li, J. Liu, T. Zhang, Single-atom catalysts: a new frontier in heterogeneous catalysis, *Acc. Chem. Res.* 46 (2013) 1740–1748, <https://doi.org/10.1021/ar300361m>.
- [26] Y. Chen, S. Ji, C. Chen, Q. Peng, D. Wang, Y. Li, Single-atom catalysts: synthetic strategies and electrochemical applications, *Joule* 2 (2018) 1242–1264, <https://doi.org/10.1016/j.joule.2018.06.019>.
- [27] W. Zhang, Y. Chao, W. Zhang, J. Zhou, F. Lv, K. Wang, F. Lin, H. Luo, J. Li, M. Tong, Emerging dual-atomic-site catalysts for efficient energy catalysis, *Adv. Mater.* 33 (2021) 2102576, <https://doi.org/10.1002/adma.202102576>.
- [28] Z. Lei, C. Sathish, Y. Liu, A. Karokoti, J. Wang, L. Qiao, A. Vinu, J. Yi, Single metal atoms catalysts—promising candidates for next generation energy storage and conversion devices, *EcoMat* 4 (2022) e12186, <https://doi.org/10.1002/eom.212186>.
- [29] A. Pedersen, J. Barrio, A. Li, R. Jervis, D.J. Brett, M.M. Titirici, I.E. Stephens, Dual-metal atom electrocatalysts: theory, synthesis, characterization, and applications, *Adv. Energy Mater.* 12 (2022) 2102715, <https://doi.org/10.1002/aenm.202102715>.
- [30] J. Zhang, Q.-a. Huang, J. Wang, J. Zhang, Y. Zhao, Supported dual-atom catalysts: preparation, characterization, and potential applications, *Chin. J. Catal.* 41 (2020) 783–798, [https://doi.org/10.1016/S1872-2067\(20\)63536-7](https://doi.org/10.1016/S1872-2067(20)63536-7).
- [31] R. Li, D. Wang, Superiority of dual-atom catalysts in electrocatalysis: one step further than single-atom catalysts, *Adv. Energy Mater.* 12 (2022) 2103564, <https://doi.org/10.1002/aenm.202103564>.
- [32] S. Zhang, M. Hou, Y. Zhai, H. Liu, D. Zhai, Y. Zhu, L. Ma, B. Wei, J. Huang, Dual-active-sites single-atom catalysts for advanced applications, *Small* 19 (2023) 2302739, <https://doi.org/10.1002/smll.202302739>.
- [33] W. Xu, Y. Wang, C. Zhang, X. Ma, J. Wu, Y. Liu, B. Lu, H. Zhang, C. Ming, J. Xiang, Insights into the electronic structure coupling effect of dual-metal atomic electrocatalytic platform for efficient clean energy conversion, *Chem. Eng. J.* 461 (2023) 141911, <https://doi.org/10.1016/j.cej.2023.141911>.
- [34] Y. Chen, J. Lin, Q. Pan, X. Liu, T. Ma, X. Wang, Inter-metal interaction of dual-atom catalysts in heterogeneous catalysis, *Angew. Chem. Int. Ed. Engl.* 62 (2023) e202306469, <https://doi.org/10.1002/anie.202306469>.
- [35] Y. Ying, X. Luo, J. Qiao, H. Huang, “More is different:” synergistic effect and structural engineering in double-atom catalysts, *Adv. Funct. Mater.* 31 (2021) 2007423, <https://doi.org/10.1002/adfm.202007423>.
- [36] Y. Wang, Q. Cao, C. Guan, C. Cheng, Recent advances on self-supported arrayed bifunctional oxygen electrocatalysts for flexible solid-state Zn-air batteries, *Small* 16 (2020) 2002902, <https://doi.org/10.1002/smll.202002902>.

- [37] J. Park, M. Park, G. Nam, J.s. Lee, J. Cho, All-solid-state cable-type flexible zinc-air battery, *Adv. Mater.* 27 (2015) 1396–1401, <https://doi.org/10.1002/adma.201404639>.
- [38] S.S. Shinde, J.Y. Jung, N.K. Wagh, C.H. Lee, D.-H. Kim, S.-H. Kim, S.U. Lee, J.-H. Lee, Ampere-hour-scale zinc-air pouch cells, *Nat. Energy* 6 (2021) 592–604, <https://doi.org/10.1038/s41560-021-00807-8>.
- [39] L. Li, A. Manthiram, Long-life, high-voltage acidic Zn-air batteries, *Adv. Energy Mater.* 6 (2016) 1502054, <https://doi.org/10.1002/aenm.201502054>.
- [40] C. Wang, J. Li, Z. Zhou, Y. Pan, Z. Yu, Z. Pei, S. Zhao, L. Wei, Y. Chen, Rechargeable zinc-air batteries with neutral electrolytes: recent advances, challenges, and prospects, *Inside Energy* 3 (2021) 100055, <https://doi.org/10.1016/j.jenchem.2021.100055>.
- [41] Z. Zhao, X. Fan, J. Ding, W. Hu, C. Zhong, J. Lu, Challenges in zinc electrodes for alkaline zinc-air batteries: obstacles to commercialization, *ACS Energy Lett.* 4 (2019) 2259–2270, <https://doi.org/10.1021/acsenergylett.9b01541>.
- [42] Z. Chen, Q. Wang, X. Zhang, Y. Lei, W. Hu, Y. Luo, Y. Wang, N-doped defective carbon with trace Co for efficient rechargeable liquid electrolyte-all-solid-state Zn-air batteries, *Sci. Bull.* 63 (2018) 548–555, <https://doi.org/10.1016/j.scib.2018.04.003>.
- [43] Q. Zhang, J. Guan, Applications of atomically dispersed oxygen reduction catalysts in fuel cells and zinc-air batteries, *Energy Environ. Mater.* 4 (2021) 307–335, <https://doi.org/10.1002/eem.21218>.
- [44] D. Stock, S. Dongmo, F. Walther, J. Sann, J.r. Janek, D. Schröder, Homogeneous coating with an anion-exchange ionomer improves the cycling stability of secondary batteries with zinc anodes, *ACS Appl. Mater. Interfaces* 10 (2018) 8640–8648, <https://doi.org/10.1021/acsmami.7b18623>.
- [45] J. Zhang, Q. Zhou, Y. Tang, L. Zhang, Y. Li, J. Zhang, Zinc-air batteries: are they ready for prime time? *Chem. Sci.* 10 (2019) 8924–8929, <https://doi.org/10.1039/C9SC04221K>.
- [46] H.-W. Liang, X. Zhuang, S. Brüller, X. Feng, K. Müllen, Hierarchically porous carbons with optimized nitrogen doping as highly active electrocatalysts for oxygen reduction, *Nat. Commun.* 5 (2014) 4973, <https://doi.org/10.1038/ncomms5973>.
- [47] N.-T. Stuen, S.-F. Hung, Q. Quan, N. Zhang, Y.-J. Xu, H.M. Chen, Electrocatalysis for the oxygen evolution reaction: recent development and future perspectives, *Chem. Soc. Rev.* 46 (2017) 337–365, <https://doi.org/10.1039/C6CS00328A>.
- [48] Z. Shi, Y. Wang, J. Li, X. Wang, Y. Wang, Y. Li, W. Xu, Z. Jiang, C. Liu, W. Xing, Confined Ir single sites with triggered lattice oxygen redox: toward boosted and sustained water oxidation catalysis, *Joule* 5 (2021) 2164–2176, <https://doi.org/10.1016/j.joule.2021.05.018>.
- [49] J. Rossmeisl, Z.W. Qu, H. Zhu, G.J. Kroes, J.K. Nørskov, Electrolysis of water on oxide surfaces, *J. Electroanal. Chem.* 607 (2007) 83–89, <https://doi.org/10.1016/j.jelechem.2006.11.008>.
- [50] D. Liu, Y. Tong, X. Yan, J. Liang, S.X. Dou, Recent advances in carbon-based bifunctional oxygen catalysts for zinc-air batteries, *Batteries Supercaps* 2 (2019) 743–765, <https://doi.org/10.1002/batt.201900052>.
- [51] J. Zhang, J. Lian, Q. Jiang, G. Wang, Boosting the OER/ORR/HER activity of Ru-doped Ni/Co oxides heterostructure, *Chem. Eng. J.* 439 (2022) 135634, <https://doi.org/10.1016/j.cej.2022.135634>.
- [52] J. Wang, C.-X. Zhao, J.-N. Liu, Y.-W. Song, J.-Q. Huang, B.-Q. Li, Dual-atom catalysts for oxygen electrocatalysis, *Nano Energy* 104 (2022) 107927, <https://doi.org/10.1016/j.nanoen.2022.107927>.
- [53] W. Lei, Y.-P. Deng, G. Li, Z.P. Cano, X. Wang, D. Luo, Y. Liu, D. Wang, Z. Chen, Two-dimensional phosphorus-doped carbon nanosheets with tunable porosity for oxygen reactions in zinc-air batteries, *ACS Catal.* 8 (2018) 2464–2472, <https://doi.org/10.1021/acscatal.7b02739>.
- [54] S. Wang, S. Chen, L. Ma, J.A. Zapien, Recent progress in cobalt-based carbon materials as oxygen electrocatalysts for zinc-air battery applications, *Mater. Today Energy* 20 (2021) 100659, <https://doi.org/10.1016/j.mtener.2021.100659>.
- [55] A. Alabdai, C. Wang, R.A. Adomaitis, Mechanism and kinetics of HER and OER on NiFe LDH Films in an alkaline electrolyte, *J. Electrochem. Soc.* 165 (2018) J3395–J3404, <https://doi.org/10.1149/2.0481815jes>.
- [56] S. Hu, G. He, H. Liu, X. Kang, Q. Yu, B. Liu, Low-dimensional electrocatalysts for acidic oxygen evolution: intrinsic activity, high current density operation, and long-term stability, *Adv. Funct. Mater.* 32 (2022) 2201726, <https://doi.org/10.1002/adfm.202201726>.
- [57] H.-F. Wang, Q. Xu, Materials design for rechargeable metal-air batteries, *Matter* 1 (2019) 565–595, <https://doi.org/10.1016/j.matt.2019.05.008>.
- [58] M.N. Masri, A.A. Mohamad, Effect of adding carbon black to a porous zinc anode in a zinc-air battery, *J. Electrochem. Soc.* 160 (2013) A715, <https://doi.org/10.1149/2.007306jes>.
- [59] L. Liu, A. Corma, Metal catalysts for heterogeneous catalysis: from single atoms to Nanoclusters and nanoparticles, *Chem. Rev.* 118 (2018) 4981–5079, <https://doi.org/10.1021/acs.chemrev.7b00776>.
- [60] S. Wang, L. Shi, X. Bai, Q. Li, C. Ling, J. Wang, Highly efficient photo-/electrocatalytic reduction of nitrogen into ammonia by dual-metal sites, *ACS Cent. Sci.* 6 (2020) 1762–1771, <https://doi.org/10.1021/acscentsci.0c00552>.
- [61] H. Zhang, X. Jin, J.-M. Lee, X. Wang, Tailoring of active sites from single to dual atom sites for highly efficient electrocatalysis, *ACS Nano* 16 (2022) 17572–17592, <https://doi.org/10.1021/acsnano.2c06827>.
- [62] J. Kim, S. Choi, J. Cho, S.Y. Kim, H.W. Jang, Toward multicomponent single-atom catalysis for efficient electrochemical energy conversion, *ACS Mater. Au.* 2 (2021) 1–20, <https://doi.org/10.1021/acsmaterialsau.1c00041>.
- [63] X. Zhang, Z. Zhu, Y. Tan, K. Qin, F.-X. Ma, J. Zhang, Co, Fe codoped holey carbon nanosheets as bifunctional oxygen electrocatalysts for rechargeable Zn-air batteries, *Commun. Chem.* 57 (2021) 2049–2052, <https://doi.org/10.1039/DCCO07767D>.
- [64] Y.-j. Wu, X.-h. Wu, T.-x. Tu, P.-f. Zhang, J.-t. Li, Y. Zhou, L. Huang, S.-g. Sun, Controlled synthesis of $\text{FeN}_x\text{-CoN}_x$ dual active sites interfaced with metallic Co nanoparticles as bifunctional oxygen electrocatalysts for rechargeable Zn-air batteries, *Appl. Catal., B* 278 (2020) 119259, <https://doi.org/10.1016/j.apcatb.2020.119259>.
- [65] Y. Wang, G. Zhang, M. Ma, Y. Ma, J. Huang, C. Chen, Y. Zhang, X. Sun, Z. Yan, Ultrasmall NiFe layered double hydroxide strongly coupled on atomically dispersed FeCo-NC nanoflowers as efficient bifunctional catalyst for rechargeable Zn-air battery, *Sci. China Mater.* 63 (2020) 1182–1195, <https://doi.org/10.1007/s40843-020-1276-8>.
- [66] Y. Luo, J. Zhang, J. Chen, Y. Chen, C. Zhang, Y. Luo, G. Wang, R. Wang, Bi-functional electrocatalysis through synergistic coupling strategy of atomically dispersed Fe and Co active sites anchored on 3D nitrogen-doped carbon sheets for Zn-air battery, *J. Catal.* 397 (2021) 223–232, <https://doi.org/10.1016/j.jcat.2021.03.030>.
- [67] Y. Wang, H. Su, Y. He, L. Li, S. Zhu, H. Shen, P. Xie, X. Fu, G. Zhou, C. Feng, Advanced electrocatalysts with single-metal-atom active sites, *Chem. Rev.* 120 (2020) 12217–12314, <https://doi.org/10.1021/acs.chemrev.0c00594>.
- [68] P. Tieu, X. Yan, M. Xu, P. Christopher, X. Pan, Directly probing the local coordination, charge state, and stability of single atom catalysts by advanced electron microscopy: a review, *Small* 17 (2021) 2006482, <https://doi.org/10.1002/smll.202006482>.
- [69] A. Pedersen, J. Barrio, A. Li, R. Jervis, D.J. Brett, M.M. Titirici, I.E. Stephens, Dual-metal atom electrocatalysts: theory, synthesis, characterization, and applications, *Adv. Energy Mater.* 12 (2022) 2102715, <https://doi.org/10.1002/aenm.202102715>.
- [70] A.M. Roth-Zawadzki, A.J. Nielsen, R.E. Tankard, J. Kibsgaard, Dual and Triple atom electrocatalysts for energy conversion (CO₂RR, NRR, ORR, OER, and HER): synthesis, characterization, and activity evaluation, *ACS Catal.* 14 (2024) 1121–1145, <https://doi.org/10.1021/acscatal.3c05000>.
- [71] L. Jiao, J. Zhu, Y. Zhang, W. Yang, S. Zhou, A. Li, C. Xie, X. Zheng, W. Zhou, S.-H. Yu, H.-L. Jiang, Non-bonding interaction of neighboring Fe and Ni single-atom pairs on MOF-derived N-doped carbon for enhanced CO₂ Electroreduction, *J. Am. Chem. Soc.* 143 (2021) 19417–19424, <https://doi.org/10.1021/jacs.1c08050>.
- [72] A.J. Frenkel, Applications of extended X-ray absorption fine-structure spectroscopy to studies of bimetallic nanoparticle catalysts, *Chem. Soc. Rev.* 41 (2012) 8163–8178.
- [73] J. Du, G. Han, W. Zhang, L. Li, Y. Yan, Y. Shi, X. Zhang, L. Geng, Z. Wang, Y. Xiong, G. Yin, C. Du, CoIn dual-atom catalyst for hydrogen peroxide production via oxygen reduction reaction in acid, *Nat. Commun.* 14 (2023) 4766, <https://doi.org/10.1038/s41467-023-40467-8>.
- [74] X. Zhang, X. Zhu, S. Bo, C. Chen, M. Qiu, X. Wei, N. He, C. Xie, W. Chen, J. Zheng, Identifying and tailoring C–N coupling site for efficient urea synthesis over diatomic Fe–Ni catalyst, *Nat. Commun.* 13 (2022) 5337, <https://doi.org/10.1038/s41467-022-33066-6>.
- [75] N. Zhang, X. Zhang, Y. Kang, C. Ye, R. Jin, H. Yan, R. Lin, J. Yang, Q. Xu, Y. Wang, Q. Zhang, L. Gu, L. Liu, W. Song, J. Liu, D. Wang, Y. Li, A supported Pd₂ dual-atom site catalyst for efficient electrochemical CO₂ reduction, *Angew. Chem. Int. Ed. Engl.* 60 (2021) 13388–13393, <https://doi.org/10.1002/anie.202101559>.
- [76] Y.S. Wei, L. Sun, M. Wang, J. Hong, L. Zou, H. Liu, Y. Wang, M. Zhang, Z. Liu, Y. Li, Fabricating dual-atom iron catalysts for efficient oxygen evolution reaction: a heteroatom modulator approach, *Angew. Chem. Int. Ed. Engl.* 59 (2020) 16013–16022, <https://doi.org/10.1002/anie.202007221>.
- [77] M. Huang, H. Meng, J. Luo, H. Li, Y. Feng, X.-X. Xue, Understanding the activity and design principle of dual-atom catalysts supported on C₂N for oxygen reduction and evolution reactions: from homonuclear to heteronuclear, *J. Phys. Chem. Lett.* 14 (2023) 1674–1683, <https://doi.org/10.1021/acs.jpclett.2c03888>.
- [78] W. Ye, S. Chen, Y. Lin, L. Yang, S. Chen, X. Zheng, Z. Qi, C. Wang, R. Long, M. Chen, Precisely tuning the number of Fe atoms in clusters on N-doped carbon toward acidic oxygen reduction reaction, *Chem* 5 (2019) 2865–2878, <https://doi.org/10.1016/j.chempr.2019.07.020>.
- [79] H. Liu, F. Yu, K. Wu, G. Xu, C. Wu, H.-K. Liu, S.-X. Dou, Recent progress on Fe-based single/dual-atom catalysts for Zn-air batteries, *Small* 18 (2022) 2106635, <https://doi.org/10.1002/smll.202106635>.
- [80] M. Ma, A. Kumar, D. Wang, Y. Wang, Y. Jia, Y. Zhang, G. Zhang, Z. Yan, X. Sun, Boosting the bifunctional oxygen electrocatalytic performance of atomically dispersed Fe site via atomic Ni neighboring, *Appl. Catal., B* 274 (2020) 119091, <https://doi.org/10.1016/j.apcatb.2020.119091>.
- [81] M. Xiao, J. Zhu, S. Li, G. Li, W. Liu, Y.-P. Deng, Z. Bai, L. Ma, M. Feng, T. Wu, D. Su, J. Lu, A. Yu, Z. Chen, 3d-Orbital occupancy regulated Ir-Co atomic pair toward superior bifunctional oxygen electrocatalysis, *ACS Catal.* 11 (2021) 8837–8846, <https://doi.org/10.1021/acscatal.1c02165>.
- [82] Y. He, X. Yang, Y. Li, L. Liu, S. Guo, C. Shu, F. Liu, Y. Liu, Q. Tan, G. Wu, Atomically dispersed Fe–Co dual metal sites as bifunctional oxygen electrocatalysts for rechargeable and flexible Zn-air batteries, *ACS Catal.* 12 (2022) 1216–1227.
- [83] Z. Wang, C. Li, Y. Liu, Y. Wu, S. Zhang, C. Deng, Atomically dispersed Fe-Ni dual sites in heteroatom doped carbon tyres for efficient oxygen electrocatalysis in rechargeable Zn-Air battery, *J. Energy Chem.* 83 (2023) 264–274, <https://doi.org/10.1016/j.jechem.2023.03.047>.
- [84] X. Han, X. Ling, D. Yu, D. Xie, L. Li, S. Peng, C. Zhong, N. Zhao, Y. Deng, W. Hu, Atomically dispersed binary Co-Ni sites in nitrogen-doped hollow carbon nanocubes for reversible oxygen reduction and evolution, *Adv. Mater.* 31 (2019) 1905622, <https://doi.org/10.1002/adma.201905622>.

- [85] D. Zhang, L. Gong, J. Ma, X. Wang, L. Zhang, Z. Xia, Disperse multimetal atom-doped carbon as efficient bifunctional electrocatalysts for oxygen reduction and evolution reactions: design strategies, *J. Phys. Chem. C* 124 (2020) 27387–27395, <https://doi.org/10.1021/acs.jpcc.0c08692>.
- [86] X. Zhu, D. Zhang, C.-J. Chen, Q. Zhang, R.-S. Liu, Z. Xia, L. Dai, R. Amal, X. Lu, Harnessing the interplay of Fe–Ni atom pairs embedded in nitrogen-doped carbon for bifunctional oxygen electrocatalysis, *Nano Energy* 71 (2020) 104597, <https://doi.org/10.1016/j.nanoen.2020.104597>.
- [87] W. Wan, Y. Zhao, S. Wei, C.A. Triana, J. Li, A. Arcifa, C.S. Allen, R. Cao, G.R. Patzke, Mechanistic insight into the active centers of single/dual-atom Ni/Fe-based oxygen electrocatalysts, *Nat. Commun.* 12 (2021) 5589, <https://doi.org/10.1038/s41467-021-25811-0>.
- [88] X. Zhou, S. Chu, Z. Jin, K. Hu, P. Liu, H.-J. Qiu, X. Lin, Revealing the synergistic Enhancement effect of dual metal RuFe(Co) sites for bifunctional oxygen catalysis, *ACS Mater. Lett.* 5 (2023) 1656–1664, <https://doi.org/10.1021/acsmaterialslett.3c00286>.
- [89] J. Cai, Y. Xu, Y. Sun, H. Zhao, D. Ye, Y. Tang, C. Sun, L. Liu, J. Zhang, Regulating the coordination environment of Fe/Co–N/S–C to enhance ORR and OER bifunctional performance, *Inorg. Chem. Front.* 10 (2023) 1826–1837, <https://doi.org/10.1039/DQI02704F>.
- [90] H. Shi, H. Wang, Y. Zhou, J. Li, P. Zhai, X. Li, G.G. Gurzadyan, J. Hou, H. Yang, X. Guo, Atomically dispersed Indium-copper dual-metal active sites promoting C–C coupling for CO₂ Photoreduction to Ethanol, *Angew. Chem. Int. Ed. Engl.* 61 (2022) e202208904, <https://doi.org/10.1002/anie.202208904>.
- [91] Z. Yu, C. Si, A.P. LaGrow, Z. Tai, W.A. Caliebe, A. Tayal, M.J. Sampayo, J.P. Sousa, I. Amorim, A. Araujo, Iridium–iron diatomic active sites for efficient bifunctional oxygen electrocatalysis, *ACS Catal.* 12 (2022) 9397–9409, <https://doi.org/10.1021/acscatal.2c01861>.
- [92] J. Wang, W. Liu, G. Luo, Z. Li, C. Zhao, H. Zhang, M. Zhu, Q. Xu, X. Wang, C. Zhao, Synergistic effect of well-defined dual sites boosting the oxygen reduction reaction, *Energy Environ. Sci.* 11 (2018) 3375–3379, <https://doi.org/10.1039/C8EE02656D>.
- [93] M. Liu, H. Chun, T.-C. Yang, S.J. Hong, C.-M. Yang, B. Han, L.Y.S. Lee, Tuning the site-to-site interaction in Ru–M (M = Co, Fe, Ni) diatomic electrocatalysts to Climb up the volcano Plot of oxygen Electroc_reduction, *ACS Nano* 16 (2022) 10657–10666, <https://doi.org/10.1021/acsnano.2c02324>.
- [94] G. Yang, J. Zhu, P. Yuan, Y. Hu, G. Qu, B.-A. Lu, X. Xue, H. Yin, W. Cheng, J. Cheng, W. Xu, J. Li, J. Hu, S. Mu, J.-N. Zhang, Regulating the Fe-spin state by atomically dispersed Mn-N in Fe-N-C catalysts with high oxygen reduction activity, *Nat. Commun.* 12 (2021) 1734, <https://doi.org/10.1038/s41467-021-21919-5>.
- [95] T. Cui, Y.P. Wang, T. Ye, J. Wu, Z. Chen, J. Li, Y. Lei, D. Wang, Y. Li, Engineering dual single-atom sites on 2D ultrathin N-doped carbon nanosheets attaining ultra-low-temperature zinc-air battery, *Angew. Chem. Int. Ed. Engl.* 61 (2022) e202115219, <https://doi.org/10.1002/anie.202115219>.
- [96] H. Li, J. Wang, R. Qi, Y. Hu, J. Zhang, H. Zhao, J. Zhang, Y. Zhao, Enhanced Fe 3d delocalization and moderate spin polarization in FeNi atomic pairs for bifunctional ORR and OER electrocatalysis, *Appl. Catal., B* 285 (2021) 119778, <https://doi.org/10.1016/j.apcatb.2020.119778>.
- [97] X. Zhou, J. Gao, Y. Hu, Z. Jin, K. Hu, K.M. Reddy, Q. Yuan, X. Lin, H.-J. Qiu, Theoretically revealed and experimentally demonstrated synergistic electronic interaction of CoFe dual-metal sites on N-doped carbon for boosting both oxygen reduction and evolution reactions, *Nano Lett.* 22 (2022) 3392–3399, <https://doi.org/10.1021/acsnanolett.2c00658>.
- [98] Y. Ma, H. Fan, C. Wu, M. Zhang, J. Yu, L. Song, K. Li, J. He, An efficient dual-metal single-atom catalyst for bifunctional catalysis in zinc-air batteries, *Carbon* 185 (2021) 526–535, <https://doi.org/10.1016/j.carbon.2021.09.044>.
- [99] Y. Chen, J. Lin, Q. Pan, X. Liu, T. Ma, X. Wang, Inter-metal interaction of dual-atom catalysts in heterogeneous catalysis, *Angew. Chem. Int. Ed. Engl.* 62 (2023) e202306469, <https://doi.org/10.1002/ange.202306469>.
- [100] Z. Chen, X. Liao, C. Sun, K. Zhao, D. Ye, J. Li, G. Wu, J. Fang, H. Zhao, J. Zhang, Enhanced performance of atomically dispersed dual-site Fe-Mn electrocatalysts through cascade reaction mechanism, *Appl. Catal., B* 288 (2021) 120021, <https://doi.org/10.1016/j.apcatb.2021.120021>.
- [101] J. Chen, H. Li, C. Fan, Q. Meng, Y. Tang, X. Qiu, G. Fu, T. Ma, Dual single-atomic Ni-N₄ and Fe-N₄ sites constructing Janus hollow graphene for selective oxygen electrocatalysis, *Adv. Mater.* 32 (2020) 2003134, <https://doi.org/10.1002/adma.202003134>.
- [102] S. Sarkar, A. Biswas, E.E. Siddharthan, R. Thapa, R.S. Dey, Strategic modulation of Target-specific isolated Fe,Co single-atom active sites for oxygen electrocatalysis impacting high power Zn-air battery, *ACS Nano* 16 (2022) 7890–7903, <https://doi.org/10.1021/acsnano.2c00547>.
- [103] C. Hu, Y. Wang, J. Chen, H.F. Wang, K. Shen, K. Tang, L. Chen, Y. Li, Main-group metal single-atomic Regulators in dual-metal catalysts for enhanced electrochemical CO₂ reduction, *Small* 18 (2022) 2201391, <https://doi.org/10.1002/smll.202201391>.
- [104] A. Han, X. Wang, K. Tang, Z. Zhang, C. Ye, K. Kong, H. Hu, L. Zheng, P. Jiang, C. Zhao, An adjacent atomic platinum site enables single-atom iron with high oxygen reduction reaction performance, *Angew. Chem. Int. Ed. Engl.* 60 (2021) 19262–19271, <https://doi.org/10.1002/anie.202105186>.
- [105] M. Liu, N. Li, S. Cao, X. Wang, X. Lu, L. Kong, Y. Xu, X.H. Bu, A “Pre-constrained metal twins” strategy to prepare efficient dual-metal-atom catalysts for cooperative oxygen electrocatalysis, *Adv. Mater.* 34 (2022) 2107421, <https://doi.org/10.1002/adma.202107421>.
- [106] S. Wang, Z. Li, W. Duan, P. Sun, J. Wang, Q. Liu, L. Zhang, Y. Zhuang, Conjugated polymerized bimetallic phthalocyanine based electrocatalyst with Fe–N₄/Co–N₄ dual-sites synergistic effect for zinc-air battery, *J. Energy Chem.* 86 (2023) 41–53, <https://doi.org/10.1016/j.jechem.2023.07.009>.
- [107] S.S. Shinde, C.H. Lee, J.-Y. Jung, N.K. Wagh, S.-H. Kim, D.-H. Kim, C. Lin, S.U. Lee, J.-H. Lee, Unveiling dual-linkage 3D hexaiminobenzene metal–organic frameworks towards long-lasting advanced reversible Zn–air batteries, *Energy Environ. Sci.* 12 (2019) 727–738, <https://doi.org/10.1039/C8EE02679C>.
- [108] S. Chen, B. Gong, J. Gu, Y. Lin, B. Yang, Q. Gu, R. Jin, Q. Liu, W. Ying, X. Shi, W. Xu, L. Cai, Y. Li, Z. Sun, S. Wei, W. Zhang, J. Lu, Dehydrogenation of ammonia Borane by platinum-nickel dimers: regulation of heteroatom Interspace Boosts bifunctional synergistic catalysis, *Angew. Chem. Int. Ed.* 61 (2022) e202211919, <https://doi.org/10.1002/anie.202211919>.
- [109] L. Shen, Y.-W. Song, J. Wang, C.-X. Zhao, C.-X. Bi, S.-Y. Sun, X.-Q. Zhang, B.-Q. Li, Q. Zhang, Synergistic catalysis on dual-atom sites for high-performance lithium–sulfur batteries, *Small Struct* 4 (2023) 2200205, <https://doi.org/10.1002/sstr.202200205>.
- [110] R. Li, J. Zhao, B. Liu, D. Wang, Atomic distance engineering in metal catalysts to regulate catalytic performance, *Adv. Mater.* (2023) 2308653, <https://doi.org/10.1002/adma.202308653>.
- [111] J. Shan, C. Ye, Y. Jiang, M. Jaroniec, Y. Zheng, S.-Z. Qiao, Metal–metal interactions in correlated single-atom catalysts, *Sci. Adv.* 8 (2022), <https://doi.org/10.1126/sciadv.abo0762> eab0762.
- [112] H.-S. Fan, X. Liang, F.-X. Ma, G. Zhang, Z.-Q. Liu, L. Zhen, X.C. Zeng, C.-Y. Xu, Low-potential iodide oxidation enables dual-atom CoFe–N–C catalysts for ultra-stable and high-energy-efficiency Zn–air batteries, *Small* (2023) 2307863, <https://doi.org/10.1002/smll.202307863>.
- [113] G. Yasin, S. Ali, S. Ibraheem, A. Kumar, M. Tabish, M.A. Mushtaq, S. Ajmal, M. Arif, M.A. Khan, A. Saad, L. Qiao, W. Zhao, Simultaneously engineering the synergistic-effects and coordination-environment of dual-single-atomic iron/cobalt-sites as a bifunctional oxygen electrocatalyst for rechargeable zinc-air batteries, *ACS Catal.* 13 (2023) 2313–2325, <https://doi.org/10.1021/acscatal.2c05654>.
- [114] R. Li, P. Rao, D. Wu, J. Li, P. Deng, Z. Miao, X. Tian, Understanding the bifunctional Trends of Fe-based binary single-atom catalysts, *Adv. Sci.* 10 (2023) 2301566, <https://doi.org/10.1002/advs.202301566>.
- [115] Z. Li, S. Ji, C. Wang, H. Liu, L. Leng, L. Du, J. Gao, M. Qiao, J.H. Horton, Y. Wang, Geometric and electronic engineering of atomically dispersed copper-cobalt diatomic sites for synergistic promoting bifunctional oxygen electrocatalysis in zinc-air batteries, *Adv. Mater.* (2023) 2300905, <https://doi.org/10.1002/adma.202300905>.
- [116] X. Wang, L. Xu, C. Li, C. Zhang, H. Yao, R. Xu, P. Cui, X. Zheng, M. Gu, J. Lee, H. Jiang, M. Huang, Developing a class of dual atom materials for multifunctional catalytic reactions, *Nat. Commun.* 14 (2023) 7210, <https://doi.org/10.1038/s41467-023-42756-8>.
- [117] D. Yu, Y. Ma, F. Hu, C.-C. Lin, L. Li, H.-Y. Chen, X. Han, S. Peng, Dual-sites coordination engineering of single atom catalysts for flexible metal–air batteries, *Adv. Energy Mater.* 11 (2021) 2101242, <https://doi.org/10.1002/adem.202101242>.
- [118] Y. Chen, S. Qiao, Y. Tang, Y. Du, D. Zhang, W. Wang, H. Zhang, X. Sun, C. Liu, Double-faced atomic-level engineering of hollow carbon Nanofibers as free-Standing bifunctional oxygen electrocatalysts for flexible Zn–air battery, *ACS Nano* 16 (2022) 15273–15285, <https://doi.org/10.1021/acsnano.2c06700>.
- [119] Y. Wang, Z. Li, P. Zhang, Y. Pan, Y. Zhang, Q. Cai, S.R.P. Silva, J. Liu, G. Zhang, X. Sun, Z. Yan, Flexible carbon nanofiber film with diatomic Fe-Co sites for efficient oxygen reduction and evolution reactions in wearable zinc-air batteries, *Nano Energy* 87 (2021) 106147, <https://doi.org/10.1016/j.nanoen.2021.106147>.
- [120] X. Liu, Y. Liu, C. Zhang, Y. Chen, G. Luo, Z. Wang, D. Wang, S. Gao, N, S co-doped hollow carbon nanocages confined Fe, Co bimetallic sites for bifunctional oxygen electrocatalysis, *Chem. Eng. J.* 473 (2023) 145135, <https://doi.org/10.1016/j.cej.2023.145135>.
- [121] V. Jose, H. Hu, E. Edison, W. Manalastas Jr., H. Ren, P. Kidkhunthod, S. Sreejith, A. Jayakumar, J.M.V. Nsanzimana, M. Srinivasan, J. Choi, J.-M. Lee, Modulation of single atomic Co and Fe sites on hollow carbon nanospheres as oxygen electrodes for rechargeable Zn–air batteries, *Small Methods* 5 (2021) 2000751, <https://doi.org/10.1002/smtd.202000751>.
- [122] Y. Wang, S. Pan, Z. Lu, Z. Jia, J. Sun, A.L. Vasiliiev, P.J. Kulesza, X. Wang, J. Zhu, Y. Fu, Boosting bifunctional oxygen electrocatalysis with atomically dispersed Fe and Co dual-metal sites for flexible zinc-air batteries, *Chem. Eng. Sci.* 282 (2023) 119304, <https://doi.org/10.1016/j.ces.2023.119304>.
- [123] K. Su, S. Yang, A. Yang, Y. Guo, B. Liu, J. Zhu, Y. Tang, X. Qiu, Customizing the anisotropic electronic states of janus-distributive FeN₄ and NiN₄ dual-atom sites for reversible oxygen electrocatalysis, *Appl. Catal., B* 331 (2023) 122694, <https://doi.org/10.1016/j.apcatb.2023.122694>.
- [124] X. Zhang, Y. Li, M. Jiang, J. Wei, X. Ding, C. Zhu, H. He, H. Lai, J. Shi, Engineering the coordination environment in atomic Fe/Ni dual-sites for efficient oxygen electrocatalysis in Zn-air and Mg-air batteries, *Chem. Eng. J.* 426 (2021) 130758, <https://doi.org/10.1016/j.cej.2021.130758>.
- [125] F. Luo, J. Zhu, S. Ma, M. Li, R. Xu, Q. Zhang, Z. Yang, K. Qu, W. Cai, Z. Chen, Regulated coordination environment of Ni single atom catalyst toward high-efficiency oxygen electrocatalysis for rechargeable Zinc-air batteries, *Energy Stor. Mater.* 35 (2021) 723–730, <https://doi.org/10.1016/j.ensm.2020.12.006>.
- [126] N. Liu, A. Kumar, Z. Li, Z. Liu, C. Zhao, X. Meng, Y. Wang, L. Yang, G. Zhang, Atomic dual-site Ni/Co-Decorated carbon nanofiber paper for efficient O₂ electrocatalysis and flexible Zn-air battery, *Chemelectrochem* 9 (2022) e20220088, <https://doi.org/10.1002/celec.20220088>.
- [127] B. Hu, A. Huang, X. Zhang, Z. Chen, R. Tu, W. Zhu, Z. Zhuang, C. Chen, Q. Peng, Y. Li, Atomic Co/Ni dual sites with N/P-coordination as bifunctional oxygen

- electrocatalyst for rechargeable zinc-air batteries, *Nano Res.* 14 (2021) 3482–3488, <https://doi.org/10.1007/s12274-021-3535-4>.
- [128] P. Zhang, Z. Chen, N. Shang, K. Wang, Y. Zuo, M. Wei, H. Wang, D. Zhong, P. Pei, Advances in polymer electrolytes for solid-state zinc-air batteries, *Mater. Chem. Front.* 7 (2023) 3994–4018, <https://doi.org/10.1039/D3QM00337J>.
- [129] G. Chen, B. Yuan, J. Dang, L. Xia, C. Zhang, Q. Wang, H. Miao, J. Yuan, Recycling the spent $\text{LiNi}_{1-x-y}\text{Mn}_x\text{Co}_y\text{O}_2$ cathodes for high-performance electrocatalysts toward both the oxygen catalytic and Methanol oxidation reactions, *Small* (2023) 2306967, <https://doi.org/10.1002/smll.202306967>.
- [130] J. Dang, M. Yin, D. Pan, Z. Tian, G. Chen, J. Zou, H. Miao, Q. Wang, J. Yuan, Four-functional iron/copper sulfide heterostructure for alkaline hybrid zinc batteries and water splitting, *Chem. Eng. J.* 457 (2023) 141357, <https://doi.org/10.1016/j.cej.2023.141357>.
- [131] M. Yin, H. Miao, J. Dang, B. Chen, J. Zou, G. Chen, H. Li, High-performance alkaline hybrid zinc batteries with heterostructure nickel/cobalt sulfide, *J. Power Sources* 545 (2022) 231902, <https://doi.org/10.1016/j.jpowsour.2022.231902>.
- [132] B. Chen, H. Miao, M. Yin, R. Hu, L. Xia, C. Zhang, J. Yuan, Mn-based spinels evolved from layered manganese dioxides at mild temperature for the robust flexible quasi-solid-state zinc-air batteries, *Chem. Eng. J.* 417 (2021) 129179, <https://doi.org/10.1016/j.cej.2021.129179>.
- [133] H. Miao, B. Chen, S. Li, X. Wu, Q. Wang, C. Zhang, Z. Sun, H. Li, All-solid-state flexible zinc-air battery with polyacrylamide alkaline gel electrolyte, *J. Power Sources* 450 (2020) 227653, <https://doi.org/10.1016/j.jpowsour.2019.227653>.
- [134] S. Zhao, Y. Zuo, T. Liu, S. Zhai, Y. Dai, Z. Guo, Y. Wang, Q. He, L. Xia, C. Zhi, Multi-functional hydrogels for flexible zinc-based batteries working under extreme conditions, *Adv. Energy Mater.* 11 (2021) 2101749, <https://doi.org/10.1002/aenm.202101749>.
- [135] T. Gu, D. Zhang, Y. Yang, C. Peng, D. Xue, C. Zhi, M. Zhu, J. Liu, Dual-sites coordination engineering of single atom catalysts for full-temperature adaptive flexible ultralong-life solid-state Zn–Air batteries, *Adv. Funct. Mater.* 33 (2023) 2212299, <https://doi.org/10.1002/adfm.202212299>.
- [136] W.H. Li, J. Yang, D. Wang, Long-range interactions in diatomic catalysts boosting electrocatalysis, *Angew. Chem. Int. Ed. Engl.* 61 (2022) e202213318, <https://doi.org/10.1002/anie.202213318>.
- [137] P. Deng, J. Duan, F. Liu, N. Yang, H. Ge, J. Gao, H. Qi, D. Feng, M. Yang, Y. Qin, Atomic insights into synergistic Nitroarene Hydrogenation over Nanodiamond-supported Pt₁–Fe₁ dual-single-atom catalyst, *Angew. Chem. Int. Ed. Engl.* 62 (2023) e202307853, <https://doi.org/10.1002/anie.202307853>.
- [138] Y. Wang, J. Wu, S. Tang, J. Yang, C. Ye, J. Chen, Y. Lei, D. Wang, Synergistic Fe–Se atom pairs as bifunctional oxygen electrocatalysts Boost low-temperature rechargeable Zn-air battery, *Angew. Chem. Int. Ed. Engl.* 62 (2023) e202219191, <https://doi.org/10.1002/anie.202219191>.
- [139] T. Gu, D. Zhang, Y. Yang, C. Peng, D. Xue, C. Zhi, M. Zhu, J. Liu, Dual-sites coordination engineering of single atom catalysts for full-temperature adaptive flexible ultralong-life solid-state Zn–Air batteries, *Adv. Funct. Mater.* 33 (2023) 2212299, <https://doi.org/10.1002/adfm.202212299>.
- [140] Y. Chen, S. Hu, F. Nichols, F. Bridges, S. Kan, T. He, Y. Zhang, S. Chen, Carbon aerogels with atomic dispersion of binary iron–cobalt sites as effective oxygen catalysts for flexible zinc-air batteries, *J. Mater. Chem. A* 8 (2020) 11649–11655, <https://doi.org/10.1039/D0TA04633G>.
- [141] T. He, Y. Chen, Q. Liu, B. Lu, X. Song, H. Liu, M. Liu, Y.-N. Liu, Y. Zhang, X. Ouyang, S. Chen, Theory-guided regulation of FeN₄ spin state by neighboring Cu atoms for enhanced oxygen reduction electrocatalysis in flexible metal–air batteries, *Angew. Chem. Int. Ed. Engl.* 61 (2022) e202201007, <https://doi.org/10.1002/anie.202201007>.
- [142] Y. Gao, B. Liu, D. Wang, Microenvironment engineering of single/dual-atom catalysts for electrocatalytic application, *Adv. Mater.* 35 (2023) 2209654, <https://doi.org/10.1002/adma.202209654>.
- [143] M. Tong, F. Sun, G. Xing, C. Tian, L. Wang, H. Fu, Potential Dominates structural Recombination of single atom Mn sites for promoting oxygen reduction reaction, *Angew. Chem. Int. Ed. Engl.* (2023) e202314933, <https://doi.org/10.1002/anie.202314933>.
- [144] S. Meng, G. Li, P. Wang, M. He, X. Sun, Z. Li, S. Meng, Rare earth-based MOFs for photo/electrocatalysis, *Mater. Chem. Front.* 7 (2023) 806–827, <https://doi.org/10.1039/D2QM01201D>.
- [145] X. Wang, Y. Zhu, H. Li, J.-M. Lee, Y. Tang, G. Fu, Rare-earth single-atom catalysts: a new frontier in photo/electrocatalysis, *Small Methods* 6 (2022) 2200413, <https://doi.org/10.1002/smtd.202200413>.
- [146] D. Qiu, B. Li, C. Zhao, J. Dang, G. Chen, H. Qiu, H. Miao, A review on zinc electrodes in alkaline electrolyte: current challenges and optimization strategies, *Energy Stor. Mater.* 61 (2023) 102903, <https://doi.org/10.1016/j.ensm.2023.102903>.